Monthly Notices of the ROYAL ASTRONOMICAL SOCIETY

MNRAS **487,** 1886–1904 (2019)
Advance Access publication 2019 May 17

doi:10.1093/mnras/stz1358

Optical and UV studies of type Ia supernovae SN 2009ig and SN 2012cg

N. K. Chakradhari,[1]† D. K. Sahu[2]⋆ and G. C. Anupama[2]

[1]*School of Studies in Physics & Astrophysics, Pt. Ravishankar Shukla University, Raipur 492010, India*
[2]*Indian Institute of Astrophysics, Koramangala, Bangalore 560034, India*

Accepted 2019 May 10. Received 2019 April 19; in original form 2018 August 14

ABSTRACT

We present an extensive optical–ultraviolet photometry and analysis of a series of optical spectra of type Ia supernovae SN 2009ig and SN 2012cg. The observations range from −15 to +185 d for SN 2009ig and from −14 to 316 d for SN 2012cg, with respect to maximum light in *B* band. Both SN 2009ig and SN 2012cg exhibit similar properties. They have similar decline rate parameter ($\Delta m_{15}(B)_{\rm true} = 0.92 \pm 0.04$ for SN 2009ig and 0.93 ± 0.06 for SN 2012cg) and *B* band peak absolute magnitude (-19.45 ± 0.40 mag for SN 2009ig and -19.50 ± 0.31 mag for SN 2012cg). Their early spectra show high-velocity features in Si II and Ca II lines. The strong Fe III, Si III, and weak Si II λ5972 line during pre-maximum phase are indicative of hot photosphere. The post-maximum velocity evolution shows a plateau like phase with velocities ∼13 000 km s^{-1} for SN 2009ig and ∼10 000 km s^{-1} for SN 2012cg. Both events show spectral evolution similar to normal SNe Ia and fall in LVG and Core Normal subgroup. Both have smaller strength ratio [$\mathcal{R}$(Si II) = 0.17 for SN 2009ig and 0.20 for SN 2012cg] consistent with smaller $\Delta m_{15}(B)$. Peak bolometric luminosities ($\log L^{\rm max}_{\rm bol}$) of these events are estimated as 43.17 ± 0.16 and 43.24 ± 0.11 erg s^{-1} suggesting that 0.60 ± 0.20 $M_\odot$ of ^{56}Ni was synthesized in the explosion of SN 2009ig and 0.72 ± 0.31 $M_\odot$ in SN 2012cg.

Key words: supernovae: general – supernovae: individual: SN 2009ig – supernovae: individual: SN 2012cg – galaxies: individual: NGC 1015 – galaxies: individual: NGC 4424.

1 INTRODUCTION

Type Ia supernovae (SNe) are believed to originate from the thermonuclear disruption of a white dwarf (WD) composed of carbon and oxygen (Hoyle & Fowler 1960). Their post-peak decline of the light curve, measured using the decline rate parameter $\Delta m_{15}(B)$, is found to be correlated with the luminosity of these events, making them standardizable candles for cosmological distance measurements. The observed homogeneity in SNe Ia puts a strong constraint on the progenitor models of these events. There are two competing progenitor models: (i) the single degenerate (SD) model (Whelan & Iben 1973) which involves a single WD accreting material from a non-degenerate star and (ii) the double degenerate (DD) model, which involves the merger of C–O WDs (Iben & Tutukov 1984; Webbink 1984). However, binary configuration, conditions for explosion and burning mechanisms are still under investigation (refer Hillebrandt & Niemeyer 2000; Howell 2011; Maoz, Mannucci & Nelemans 2014, for reviews) and there could be diverse progenitor system/multiple path leading to SNe Ia explosion (see Maeda & Terada 2016, for review).

An early detection and quick follow-up of these events may provide observational signatures to understand the explosion mechanism through cooling of shock heated ejecta, interaction of ejecta with a companion/circumstellar material (CSM) and mixing of ^{56}Ni in the outer ejecta (refer Kasen 2010; Piro, Chang & Weinberg 2010; Rabinak, Livne & Waxman 2012; Dessart et al. 2014; Levanon, Soker & García-Berro 2015; Piro & Morozova 2016; Levanon & Soker 2017; Noebauer et al. 2017; Maeda et al. 2018, for discussion). Such observational signatures have been observed in very few events. The earliest observation of SN 2011fe provided a tight constrain on the size of progenitor star, giving a direct confirmation that the star exploded was a compact star (Nugent et al. 2011; Bloom et al. 2012). Early UV excess emission in a subluminous type Ia event iPTF 14atg was interpreted as due to ejecta companion collision (Cao et al. 2015). Similarly, early blue bump in the light curves of SN 2017cbv was interpreted as ejecta companion interaction (Hosseinzadeh et al. 2017). Early observations of the type Ia supernova iPTF 16abc were explained as a case of interaction with nearby unbound material and/or strong ejecta mixing (Miller et al. 2018). Interestingly, early excess emission in MUSSES1604D (SN 2016jhr) was red (Jiang et al. 2017) instead of blue, hence there may be at least two distinct early populations (Stritzinger et al. 2018) and care must be taken in the interpretation of these features.

Early spectra of several SNe Ia show additional high velocity absorption features along with the photospheric component, which

⋆ E-mail: dks@iiap.res.in
† Centre for Mega Projects in Multiwavelength Astronomy, Pt. Ravishankar Shukla University Raipur.

appears as a blend or double-minima in the absorption lines. This feature is termed as high-velocity features (HVFs, Mazzali et al. 2005a; Wang et al. 2009b; Childress et al. 2013; Marion et al. 2013; Childress et al. 2014; Zhao et al. 2015).

In this paper we present results based on photometric and low-resolution spectroscopic monitoring of two type Ia SNe, SN 2009ig, and SN 2012cg, which were caught soon after explosion. SN 2009ig was discovered on 2009 August 20.48 (UT) by Kleiser et al. (2009) in a low-redshift ($z = 0.009$) galaxy NGC 1015 of type SB(r)a (source NED) and was classified as a young type Ia SN (Navasardyan, Cappellaro & Benetti 2009). Foley et al. (2012b) presented very early UV–optical photometric and spectroscopic observations of SN 2009ig. With the early-time data they determined the *B* band rise time as $t_R = 17.13 \pm 0.07$ d. Marion et al. (2013) presented analysis of spectra of SN 2009ig taken from −14 to +13 d with respect to *B*-band maximum. The HVFs in the lines of Si II, Si III, Ca II, S II, and Fe II were identified. The absorption features make a transition from detached HVFs in the very early phase (∼−14 and −13 d), to photospheric velocity feature (PVF) at around ∼−6 d.

SN 2012cg was discovered by Cenko et al. (2012) on 2012 May 17.22 (UT) in NGC 4424, a peculiar SB(s)a type galaxy having redshift of $z = 0.00146$ (Kent et al. 2008, source NED) and was classified as a very young type Ia supernova next day of discovery. Silverman et al. (2012) presented very early photometric and spectroscopic results of SN 2012cg. Using quadratically expanding fireball model they estimated a rise time of 17.3 d. Munari et al. (2013) have presented early photometric observations of SN 2012cg covering ∼−11 to +33 d. Marion et al. (2016) presented photometry and spectroscopy during ∼−17 to +22 d. The observed excess blue light during the very early phase ∼−17 to ∼−14 d, was interpreted as impact of the supernova on the non-degenerate binary companion. The mass of the main-sequence binary companion was estimated as ∼6 $M_\odot$, favouring the SD explosion model. However based on the analysis of nebular phase spectrum, X-ray data, and pre-discovery images, Shappee et al. (2018) strongly ruled out the non-degenerate companion.

This paper aims at presenting an extensive photometry at UV and optical bands along with a detailed analysis of a series of optical spectra. Our data sets are extended from early to very late phase both in photometry as well as spectroscopy, making these objects ideal templates for future studies. The layout of this paper is as follows. In Section 2, observations along with description of data reduction is presented. In Section 3, the light curves and colour curves are discussed. In Section 4, the main parameters of the SNe e.g. peak absolute magnitude, bolometric luminosity, mass of ^{56}Ni etc. are estimated. The spectral evolution and comparison with some other well-studied SNe Ia is presented in Section 5. The results are discussed in Section 6 and Section 7 summarizes the paper.

2 OBSERVATIONS AND DATA REDUCTION

2.1 Imaging

SN 2009ig and SN 2012cg were monitored in Bessell's *UBVRI* bands using Himalaya Faint Object Spectrograph Camera (HFOSC) mounted on the 2-m Himalayan Chandra Telescope (HCT) of the Indian Astronomical Observatory (IAO), Hanle, operated by the Indian Institute of Astrophysics (IIA), Bangalore, India. The observations of SN 2009ig began on 2009 August 28 and continued until 2010 March 9. Apart from the supernova frames, several calibration frames *e.g.* twilight flats and bias frames were also acquired

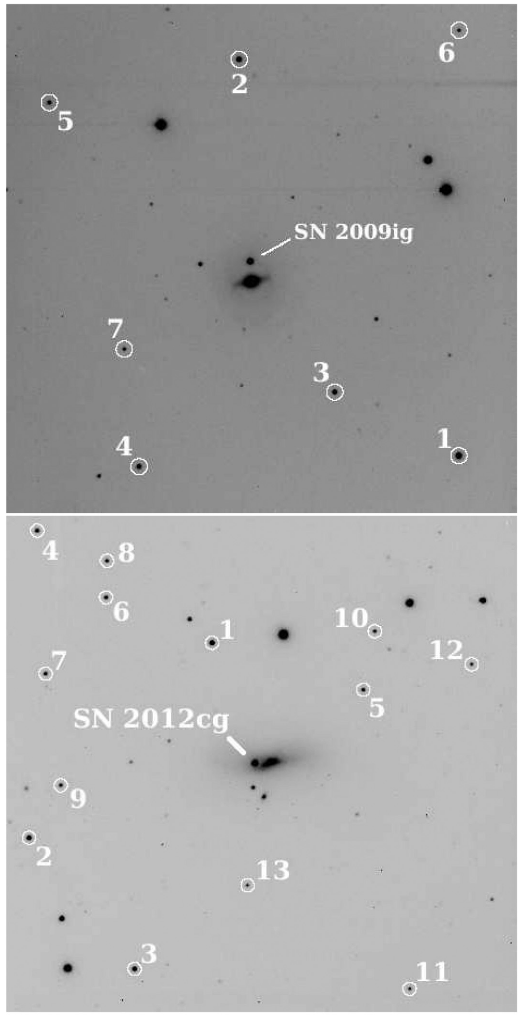

Figure 1. Identification chart for SN 2009ig (*top*) and SN 2012cg (*bottom*). The stars used as local standards are marked and their calibrated magnitudes are listed in Table 1 and 2. North is up and east to the left. The field of view is 10 × 10 arcmin^2 each.

during the observations. Standard star fields PG 0231+051, PG 1633+099, PG 2213−006 from Landolt (1992) were observed on three photometric nights, 2009 September 16, September 20, September 30, and were used to calibrate a sequence of secondary standards in the supernova field.

The photometric observations of SN 2012cg were carried out from 2012 May 20 to 2013 April 15. Standard star fields PG 1633+099, PG 2213−006, PG 0231+051 were observed on six photometric nights, 2012 May 24, June 21, June 26, July 16, 2013 January 24, and 2014 June 16. The HFOSC is equipped with a SITe CCD chip with 2K × 4K pixels. The central 2K × 2K pixels region of the chip, used in photometric observations provides a field of view of 10 × 10 arcmin^2 with a plate scale of 0.296 arcsec pixel^{-1}. The gain and readout noise of the CCD is 1.22 ele. ADU^{-1} and 4.87 ele., respectively.

Data processing was done in a standard manner using Image Reduction and Analysis Facility (IRAF[1]) package. Images were

[1] IRAF is distributed by the National Optical Astronomy Observatories, which are operated by the Association of Universities for Research in Astronomy, Inc., under cooperative agreement with the National Science Foundation.

Table 1. Magnitudes of secondary standard stars in the field of SN 2009ig. The stars are marked in Fig. 1 (top).

ID	*U*	*B*	*V*	*R*	*I*
1	15.319 ± 0.009	14.890 ± 0.030	14.110 ± 0.020	13.670 ± 0.006	13.270 ± 0.020
2	15.080 ± 0.020	15.289 ± 0.016	14.768 ± 0.009	14.390 ± 0.030	14.049 ± 0.001
3	15.650 ± 0.020	15.742 ± 0.019	15.161 ± 0.008	14.790 ± 0.030	14.457 ± 0.004
4	17.416 ± 0.014	16.502 ± 0.020	15.520 ± 0.019	14.949 ± 0.017	14.470 ± 0.020
5	16.479 ± 0.010	16.547 ± 0.015	15.960 ± 0.014	15.540 ± 0.020	15.200 ± 0.030
6	17.248 ± 0.018	17.286 ± 0.013	16.689 ± 0.008	16.320 ± 0.030	15.971 ± 0.015
7	18.423 ± 0.039	17.730 ± 0.020	16.820 ± 0.020	16.280 ± 0.030	15.795 ± 0.003

Table 2. Magnitudes of secondary standard stars in the field of SN 2012cg. The stars are marked in Fig. 1 (bottom).

ID	*U*	*B*	*V*	*R*	*I*
1	14.862 ± 0.011	15.080 ± 0.013	14.529 ± 0.018	14.165 ± 0.013	13.881 ± 0.009
2	16.352 ± 0.018	15.929 ± 0.015	15.069 ± 0.017	14.544 ± 0.016	14.098 ± 0.002
3	17.834 ± 0.031	16.699 ± 0.019	15.419 ± 0.018	14.637 ± 0.015	13.971 ± 0.006
4	16.090 ± 0.019	16.249 ± 0.012	15.661 ± 0.014	15.273 ± 0.008	14.906 ± 0.020
5	18.890 ± 0.023	17.818 ± 0.019	16.428 ± 0.013	15.457 ± 0.022	14.467 ± 0.006
6	17.440 ± 0.034	17.033 ± 0.019	16.072 ± 0.017	15.496 ± 0.014	15.007 ± 0.011
7	17.626 ± 0.014	17.061 ± 0.017	16.132 ± 0.011	15.574 ± 0.019	15.134 ± 0.004
8	16.616 ± 0.017	16.719 ± 0.010	16.095 ± 0.016	15.667 ± 0.016	15.300 ± 0.022
9	18.776 ± 0.013	17.586 ± 0.018	16.393 ± 0.018	15.695 ± 0.014	15.124 ± 0.014
10	16.609 ± 0.026	16.862 ± 0.013	16.360 ± 0.018	16.013 ± 0.023	15.709 ± 0.009
11	17.589 ± 0.018	17.369 ± 0.018	16.633 ± 0.017	16.177 ± 0.013	15.784 ± 0.016
12	17.514 ± 0.008	17.494 ± 0.018	16.733 ± 0.013	16.261 ± 0.019	15.853 ± 0.027
13	16.947 ± 0.005	17.189 ± 0.017	16.667 ± 0.015	16.304 ± 0.011	16.018 ± 0.009

Table 3. Optical *UBVRI* photometry of SN 2009ig with HCT.

Date	JD	Phase[a]	*U*	*B*	*V*	*R*	*I*
28/08/2009	245 5072.45	− 8.19	13.800 ± 0.090	14.036 ± 0.026	14.045 ± 0.012	13.950 ± 0.021	14.067 ± 0.016
01/09/2009	245 5076.45	− 4.19		13.662 ± 0.018	13.650 ± 0.019	13.644 ± 0.022	13.845 ± 0.029
05/09/2009	245 5080.32	− 0.32	13.397 ± 0.089	13.578 ± 0.018	13.511 ± 0.029	13.537 ± 0.032	13.834 ± 0.025
06/09/2009	245 5081.34	0.70	13.418 ± 0.074	13.577 ± 0.040	13.514 ± 0.024	13.500 ± 0.019	13.849 ± 0.019
12/09/2009	245 5087.38	6.74				13.682 ± 0.029	14.069 ± 0.033
13/09/2009	245 5088.27	7.63		13.861 ± 0.022	13.656 ± 0.016	13.679 ± 0.021	14.189 ± 0.039
16/09/2009	245 5091.42	10.78		14.100 ± 0.038	13.844 ± 0.022	13.911 ± 0.025	14.309 ± 0.045
20/09/2009	245 5095.35	14.71	14.250 ± 0.048	14.463 ± 0.011	14.082 ± 0.011	14.177 ± 0.028	14.520 ± 0.027
21/09/2009	245 5096.33	15.69	14.428 ± 0.042	14.555 ± 0.019	14.142 ± 0.023	14.219 ± 0.025	14.538 ± 0.025
22/09/2009	245 5097.39	16.75	14.493 ± 0.060	14.661 ± 0.021	14.162 ± 0.020	14.212 ± 0.032	14.500 ± 0.031
23/09/2009	245 5098.26	17.62	14.544 ± 0.079	14.736 ± 0.019	14.195 ± 0.020	14.265 ± 0.024	14.515 ± 0.027
24/09/2009	245 5099.25	18.61	14.713 ± 0.046	14.865 ± 0.014	14.237 ± 0.011	14.268 ± 0.017	14.488 ± 0.025
27/09/2009	245 5102.40	21.76		15.184 ± 0.012	14.330 ± 0.027	14.259 ± 0.024	14.395 ± 0.024
28/09/2009	245 5103.34	22.70	15.167 ± 0.036	15.278 ± 0.015	14.372 ± 0.021	14.250 ± 0.018	14.390 ± 0.018
30/09/2009	245 5105.27	24.63	15.280 ± 0.054	15.455 ± 0.013	14.433 ± 0.024	14.291 ± 0.023	14.353 ± 0.018
16/10/2009	245 5121.27	40.63	16.298 ± 0.076	16.384 ± 0.023	15.302 ± 0.027	14.972 ± 0.032	14.762 ± 0.034
06/11/2009	245 5142.28	61.64		16.721 ± 0.016	15.940 ± 0.021	15.760 ± 0.029	15.785 ± 0.019
13/11/2009	245 5149.16	68.52		16.856 ± 0.026	16.134 ± 0.027	15.988 ± 0.014	16.078 ± 0.021
24/11/2009	245 5160.27	79.63		17.025 ± 0.014	16.404 ± 0.024		16.462 ± 0.021
03/12/2009	245 5169.07	88.43		17.177 ± 0.035	16.646 ± 0.023	16.561 ± 0.020	16.813 ± 0.026
13/12/2009	245 5179.10	98.46	17.534 ± 0.038	17.365 ± 0.015	16.828 ± 0.010	16.851 ± 0.022	17.103 ± 0.022
20/12/2009	245 5186.03	105.39			17.065 ± 0.029	17.064 ± 0.025	17.398 ± 0.027
23/12/2009	245 5189.21	108.57	17.786 ± 0.128	17.573 ± 0.035	17.125 ± 0.018	17.162 ± 0.036	17.461 ± 0.035
29/12/2009	245 5195.06	114.42		17.634 ± 0.017	17.273 ± 0.016	17.311 ± 0.020	17.691 ± 0.016
02/01/2010	245 5199.06	118.42	18.163 ± 0.079	17.741 ± 0.017	17.331 ± 0.040	17.449 ± 0.027	17.755 ± 0.028
11/01/2010	245 5208.10	127.46	18.234 ± 0.065	17.871 ± 0.016	17.536 ± 0.018	17.676 ± 0.016	17.973 ± 0.026
20/01/2010	245 5217.10	136.46		18.038 ± 0.017	17.829 ± 0.038	17.902 ± 0.011	18.240 ± 0.020
27/01/2010	245 5224.15	143.51		18.100 ± 0.029	17.837 ± 0.054	18.065 ± 0.028	
01/02/2010	245 5229.16	148.52		18.228 ± 0.050	17.952 ± 0.034	18.211 ± 0.030	18.560 ± 0.035
27/02/2010	245 5255.42	174.78			18.265 ± 0.056	18.662 ± 0.087	
09/03/2010	245 5265.52	184.88			18.580 ± 0.034	19.008 ± 0.082	

Note: [a]Observed phase in days with respect to the epoch of *B*-band maximum: JD = 245 5080.64.

Table 4. Optical *UBVRI* photometry of SN 2012cg with HCT.

Date	JD	Phase[a]	*U*	*B*	*V*	*R*	*I*
20/05/2012	245 6068.27	– 13.73	14.500 ± 0.040	14.713 ± 0.020	14.418 ± 0.012	14.240 ± 0.034	14.225 ± 0.030
21/05/2012	245 6069.21	– 12.79	14.055 ± 0.023	14.262 ± 0.018	14.042 ± 0.024	13.848 ± 0.042	13.831 ± 0.033
22/05/2012	245 6070.11	– 11.89	13.563 ± 0.040	13.867 ± 0.034	13.685 ± 0.019	13.475 ± 0.016	13.442 ± 0.013
24/05/2012	245 6072.25	– 9.75	12.620 ± 0.061	13.130 ± 0.015	13.060 ± 0.008	12.870 ± 0.012	12.905 ± 0.022
27/05/2012	245 6075.24	– 6.76	12.100 ± 0.035	12.624 ± 0.016	12.551 ± 0.019	12.385 ± 0.007	12.419 ± 0.011
01/06/2012	245 6080.25	– 1.75	11.780 ± 0.044	12.246 ± 0.022	12.161 ± 0.018	12.073 ± 0.020	12.217 ± 0.014
03/06/2012	245 6082.22	0.22		12.223 ± 0.060	12.140 ± 0.021	12.103 ± 0.023	12.276 ± 0.027
04/06/2012	245 6083.24	1.24	11.788 ± 0.060	12.232 ± 0.019	12.064 ± 0.017	12.039 ± 0.026	12.274 ± 0.017
12/06/2012	245 6091.18	9.18	12.324 ± 0.055	12.610 ± 0.012	12.326 ± 0.014	12.270 ± 0.017	12.622 ± 0.018
18/06/2012	245 6097.21	15.21	12.988 ± 0.038	13.155 ± 0.017	12.604 ± 0.012	12.669 ± 0.035	12.861 ± 0.014
21/06/2012	245 6100.20	18.20	13.421 ± 0.019	13.558 ± 0.007	12.845 ± 0.011	12.750 ± 0.015	12.857 ± 0.016
26/06/2012	245 6105.19	23.19	14.064 ± 0.038	14.044 ± 0.033	13.054 ± 0.042	12.773 ± 0.024	12.752 ± 0.053
01/07/2012	245 6110.17	28.17	14.501 ± 0.031	14.491 ± 0.020	13.244 ± 0.022	12.879 ± 0.015	12.637 ± 0.018
06/07/2012	245 6115.20	33.20	14.823 ± 0.071	14.886 ± 0.034	13.490 ± 0.023	13.067 ± 0.031	12.698 ± 0.027
12/07/2012	245 6121.17	39.17	15.150 ± 0.027	15.148 ± 0.018		13.421 ± 0.018	13.093 ± 0.016
14/07/2012	245 6123.13	41.13	15.222 ± 0.024	15.243 ± 0.021	13.932 ± 0.012	13.552 ± 0.026	13.228 ± 0.024
15/07/2012	245 6124.18	42.18			13.982 ± 0.029	13.613 ± 0.048	13.240 ± 0.036
16/07/2012	245 6125.13	43.13	15.253 ± 0.024	15.253 ± 0.008	14.006 ± 0.016	13.642 ± 0.013	13.347 ± 0.024
29/07/2012	245 6138.11	56.11			14.416 ± 0.028	14.051 ± 0.044	
03/08/2012	245 6143.10	61.10					14.242 ± 0.042
06/08/2012	245 6146.10	64.10		15.610 ± 0.059	14.582 ± 0.049	14.390 ± 0.013	14.348 ± 0.032
30/11/2012	245 6262.45	180.45		17.384 ± 0.024	17.223 ± 0.025	17.434 ± 0.036	17.420 ± 0.040
10/01/2013	245 6302.51	220.51		17.940 ± 0.023	17.832 ± 0.020	18.189 ± 0.028	18.030 ± 0.039
15/01/2013	245 6308.41	226.41	19.448 ± 0.136	17.967 ± 0.050	17.863 ± 0.016	18.389 ± 0.024	18.026 ± 0.045
24/01/2013	245 6317.40	235.40	19.058 ± 0.234	18.238 ± 0.033	18.004 ± 0.032	18.640 ± 0.049	18.186 ± 0.052
14/02/2013	245 6338.45	256.45			18.367 ± 0.023	18.797 ± 0.030	18.454 ± 0.036
08/03/2013	245 6360.37	278.37			18.530 ± 0.025	18.978 ± 0.027	
16/03/2013	245 6368.28	286.28				19.320 ± 0.052	
15/04/2013	245 6398.34	316.34			18.987 ± 0.035	19.524 ± 0.071	19.220 ± 0.116

Note: [a]Observed phase in days with respect to the epoch of *B*-band maximum: JD = 245 6082.

bias subtracted and flat field corrected. Magnitudes of the Landolt standards were obtained by performing aperture photometry on the standards at an optimal aperture determined using the aperture growth curve, which is usually 3–4 times the full width at half maximum (FWHM) of the stellar profile in the frame. Average value of atmospheric extinction for the site and average colour terms for the system were used to determine the photometric zero-points on individual nights. A sequence of secondary standards (marked in Fig. 1) were calibrated using the average colour terms and the estimated zero-points on individual nights. The mean *UBVRI* magnitudes of secondary standards in the field of SN 2009ig and SN 2012cg are listed in Tables 1 and 2, respectively.

SN 2009ig occurred in the outer region of the host galaxy, hence profile fitting technique was adopted to estimate supernova magnitudes. The fitting radius was taken close to FWHM of the stellar profile. The difference between the aperture and profile fitting magnitudes was obtained for bright secondary standards in the field of SN 2009ig and this correction was applied to the supernova magnitude. The supernova magnitudes were calibrated differentially with respect to the local secondary standards in the field. Magnitudes of SN 2009ig obtained from the photometry of HCT data are listed in Table 3.

Since SN 2012cg occurred very close to the nucleus of host galaxy in a high-background region, the template subtraction photometry was used to extract the supernova magnitude. Deep *UBVRI* template frames of NGC 4424 field were obtained in good seeing condition with the same instrumental set-up on 2014 June 16. The template image was subtracted from the individual supernova frame. Aperture photometry was performed on supernova in the template subtracted frame and calibrated differentially with respect to the secondary standards. Supernova magnitudes derived using template subtraction photometry are listed in Table 4.

2.1.1 UV–optical photometry using Swift *UVOT*

UV–optical imaging data of SN 2009ig and SN 2012cg observed with Ultra Violet Optical Telescope (UVOT) (Roming et al. 2005) on board the *Swift* satellite (Gehrels et al. 2004) were obtained from the *Swift* archive. Images taken in the three broad-band UV filters, (*uvw*2 : 1928 Å, *uvm*2 : 2246 Å, *uvw*1 : 2600 Å) and three broad-band optical filters (*u* : 3465 Å, *b* : 4392 Å, *v* : 5468 Å) were processed using various packages in the HEASOFT (the High Energy Astrophysics Software) with latest CALDB, following methods of Poole et al. (2008) and Brown et al. (2009). SN magnitudes were obtained using *uvotsource* program. An aperture size of 5 arcsec was used for the source and similar aperture to estimate the background. During late phase when supernova became faint, magnitudes were extracted using a smaller aperture size (of 3.5–4 arcsec) and aperture corrections were applied. The UV–optical magnitudes of SN 2009ig and SN 2012cg obtained from *Swift* UVOT data are presented in Tables 5 and 6, respectively.

2.2 Spectroscopy

Medium resolution (∼7 Å) spectra of SN 2009ig and SN 2012cg were obtained using grisms Gr#7 (wavelength range 3500–7800 Å)

Table 5. UV–optical photometry of SN 2009ig with *Swift* UVOT.

JD	Phase[a]	*uvw*2	*uvm*2	*uvw*1	*u*	*b*	*v*
245 5065.34	− 15.30	20.554 ± 0.314		19.291 ± 0.198	17.695 ± 0.091	17.047 ± 0.051	16.493 ± 0.073
245 5066.55	− 14.09	19.983 ± 0.328		18.409 ± 0.178	16.583 ± 0.074	16.087 ± 0.044	15.811 ± 0.069
245 5067.08	− 13.56			17.490 ± 0.225			
245 5067.09	− 13.55	18.891 ± 0.338					
245 5068.56	− 12.08	18.463 ± 0.131		16.595 ± 0.069	14.933 ± 0.037	14.891 ± 0.029	14.860 ± 0.044
245 5069.08	− 11.56		19.764 ± 0.687	16.252 ± 0.114			
245 5069.10	− 11.54	17.999 ± 0.171					
245 5070.51	− 10.13	17.603 ± 0.086	19.062 ± 0.314	15.593 ± 0.045	14.011 ± 0.031	14.309 ± 0.027	14.281 ± 0.037
245 5070.63	− 10.01		19.167 ± 0.318				
245 5070.65	− 9.99	17.456 ± 0.151					
245 5072.97	− 7.67	16.882 ± 0.049	18.245 ± 0.141	14.950 ± 0.032	13.444 ± 0.027	13.902 ± 0.024	13.892 ± 0.030
245 5075.12	− 5.52	16.592 ± 0.043	17.955 ± 0.125	14.710 ± 0.030	13.212 ± 0.027	13.686 ± 0.024	13.726 ± 0.030
245 5075.84	− 4.80			14.662 ± 0.039			
245 5076.47	− 4.17	16.501 ± 0.072					
245 5076.59	− 4.05	16.519 ± 0.049	17.588 ± 0.124	14.667 ± 0.033	13.200 ± 0.028	13.637 ± 0.026	13.573 ± 0.031
245 5077.92	− 2.72	16.427 ± 0.072					
245 5077.94	− 2.70	16.516 ± 0.084					
245 5079.34	− 1.30	16.533 ± 0.049	17.411 ± 0.108	14.746 ± 0.033	13.265 ± 0.028	13.577 ± 0.025	13.479 ± 0.030
245 5080.54	− 0.10	16.577 ± 0.047	17.321 ± 0.102	14.819 ± 0.033	13.333 ± 0.028	13.584 ± 0.025	13.469 ± 0.030
245 5081.13	0.49				13.415 ± 0.028		
245 5081.14	0.50	16.590 ± 0.094					
245 5081.54	0.90	16.609 ± 0.076					
245 5082.54	1.90		17.427 ± 0.158				
245 5084.36	3.72	16.716 ± 0.061	17.301 ± 0.152	15.116 ± 0.041	13.571 ± 0.030	13.654 ± 0.027	13.480 ± 0.033
245 5086.70	6.06	16.951 ± 0.060	17.742 ± 0.136	15.338 ± 0.040	13.713 ± 0.030	13.737 ± 0.026	13.491 ± 0.031
245 5088.49	7.85			15.582 ± 0.062			
245 5088.51	7.87	17.189 ± 0.107					
245 5088.56	7.92				13.947 ± 0.029		
245 5089.51	8.87	17.198 ± 0.068	17.907 ± 0.144	15.637 ± 0.045	14.033 ± 0.031	13.923 ± 0.026	13.631 ± 0.031
245 5098.94	18.30	18.361 ± 0.130	19.018 ± 0.261	16.785 ± 0.079	15.175 ± 0.041	14.741 ± 0.029	14.127 ± 0.035
245 5101.81	21.17			17.087 ± 0.109			
245 5105.83	25.19	18.715 ± 0.227	19.477 ± 0.675	17.522 ± 0.182	15.926 ± 0.079	15.397 ± 0.047	14.365 ± 0.051
245 5107.84	27.20	18.978 ± 0.260	19.552 ± 0.643	17.734 ± 0.185	16.091 ± 0.084	15.564 ± 0.049	14.518 ± 0.052
245 5113.79	33.15	19.250 ± 0.216	20.111 ± 0.472	17.932 ± 0.144	16.519 ± 0.074	15.976 ± 0.044	14.827 ± 0.046
245 5116.87	36.23	19.304 ± 0.201		18.326 ± 0.184	16.602 ± 0.072	16.101 ± 0.045	15.097 ± 0.048

Note: [a]Observed phase in days with respect to the epoch of *B*-band maximum: JD = 245 5080.64.

and Gr#8 (5200–9200 Å) available with HFOSC. The journals of spectroscopic observations are given in Table 7 (for SN 2009ig) and in Table 8 (for SN 2012cg). Arc lamp spectra of FeNe and FeAr were obtained for wavelength calibration. Spectra of spectrophotometric standards were taken for correcting the instrumental response and flux calibration. Spectroscopic reductions were done in a standard manner using IRAF. The one-dimensional spectra were extracted from the bias subtracted and flat-field corrected images using the optimal extraction method. Wavelength calibration was performed using the spectra of FeAr and FeNe sources. The wavelength calibration was checked with the help of sky emission lines present in the object spectrum, and wherever necessary, a constant shift was applied to the spectrum. The wavelength calibrated spectra were corrected for instrumental response using spectra of spectrophotometric standards observed on the same night and brought to a flux scale. When we did not have standard stars observed on the same night, the response curve generated on the nearby night was used for this purpose. The flux calibrated spectra in the two different regions were combined, scaled to a weighted mean, to give the final spectrum on a relative flux scale. The reduced spectra were then brought to an absolute flux scale by applying zero-point corrections obtained from *UBVRI* photometry. Finally the spectra were reddening (refer Section 4.1) and redshift (obtained from NED) corrected.

3 LIGHT CURVES AND COLOUR CURVES

The estimated *UBVRI* and UV–optical magnitudes are plotted in Figs 2 and 3. Various photometric parameters were derived from the observed data points and are listed in Tables 9 and 10. In both the cases the pre-maximum phase is nicely covered. The date of maximum and magnitude at maximum have been estimated by fitting cubic spline function to the data points around maximum. The light-curve fit indicates that SN 2009ig reached maximum light in *B* band on JD 245 5080.64 ± 0.42 with a magnitude of 13.56 ± 0.04 mag, and thus our photometry covers −8 to +185 d with respect to the maximum in *B* band.

The post-maximum decline rate during the first 15 d in *B* band is estimated as $\Delta m_{15}(B) = 0.91 \pm 0.04$. The date of maximum, magnitude at *B*-band maximum and the decline rate $\Delta m_{15}(B)$ are consistent with the values presented by Foley et al. (2012b). The reddening (refer Section 4.1) corrected decline rate parameter $\Delta m_{15}(B)_{\rm true}$ (Phillips et al. 1999) obtained using the relation of Folatelli et al. (2010) is $\Delta m_{15}(B)_{\rm true} = 0.92$. Decline rate in different bands during (20–40 d), (50–100 d), and (100–150 d) with respect to *B*-band maximum are also estimated by fitting linear least square and the values are listed in Table 9.

SN 2012cg reached to *B*-band maximum on JD 2456082 ± 0.08. This estimate is consistent with Marion et al. (2016). The $\Delta m_{15}(B)$

Table 6. UV–optical photometry of SN 2012cg with *Swift* UVOT.

JD	Phase[a]	*uvw*2	*uvm*2	*uvw*1	*u*	*b*	*v*
245 6067.54	− 14.46	17.761 ± 0.154		16.576 ± 0.105	15.083 ± 0.062	14.827 ± 0.043	14.593 ± 0.063
245 6070.54	− 11.46		18.236 ± 0.311				
245 6070.56	− 11.44	16.717 ± 0.091					
245 6071.82	− 10.18	16.153 ± 0.044	17.416 ± 0.084	14.575 ± 0.032	12.898 ± 0.029	13.206 ± 0.028	13.033 ± 0.031
245 6073.68	− 8.32			13.876 ± 0.058			
245 6073.95	− 8.05				12.216 ± 0.056	12.884 ± 0.059	
245 6074.35	− 7.65					12.790 ± 0.044	
245 6074.48	− 7.52						12.551 ± 0.040
245 6074.55	− 7.45		16.708 ± 0.090				
245 6073.70	− 8.30	15.711 ± 0.056					
245 6075.69	− 6.31	15.350 ± 0.036	16.555 ± 0.057	13.560 ± 0.026	11.966 ± 0.035	12.626 ± 1.108	12.371 ± 0.031
245 6079.43	− 2.57	15.110 ± 0.038	16.355 ± 0.066	13.333 ± 0.028	11.850 ± 1.096		12.118 ± 0.033
245 6081.18	− 0.82				11.842 ± 1.091		12.089 ± 0.053
245 6080.84	− 1.16	15.148 ± 0.036	16.265 ± 0.056	13.375 ± 0.027	11.846 ± 1.096		12.099 ± 0.032
245 6082.91	0.91				11.883 ± 0.068		12.066 ± 0.053
245 6082.99	0.99	15.168 ± 0.030	16.316 ± 0.043	13.465 ± 0.024	11.848 ± 1.096		12.042 ± 0.028
245 6085.20	3.20				12.083 ± 0.060		12.041 ± 0.053
245 6084.58	2.58	15.240 ± 0.034	16.308 ± 0.054	13.580 ± 0.027	11.971 ± 0.034		12.034 ± 0.031
245 6086.85	4.85	15.400 ± 0.035	16.430 ± 0.053	13.801 ± 0.027	12.192 ± 0.031		12.041 ± 0.030
245 6086.92	4.92				12.226 ± 0.057		11.997 ± 0.053
245 6088.72	6.72				12.331 ± 0.055	12.642 ± 1.118	12.214 ± 0.053
245 6088.73	6.73	15.505 ± 0.044	16.632 ± 0.082	13.990 ± 0.032	12.385 ± 0.035	12.629 ± 1.107	12.074 ± 0.034
245 6094.74	12.74	16.102 ± 0.042	17.048 ± 0.072	14.679 ± 0.032	13.058 ± 0.029	12.880 ± 0.029	12.378 ± 0.029
245 6096.88	14.88	16.363 ± 0.052	17.174 ± 0.075	14.935 ± 0.040			
245 6098.61	16.61	16.604 ± 0.069	17.565 ± 0.101	15.180 ± 0.058			
245 6100.56	18.56	16.711 ± 0.059	17.628 ± 0.086	15.376 ± 0.047			
245 6103.43	21.43	17.016 ± 0.072	17.964 ± 0.120	15.678 ± 0.057			
245 6107.64	25.64	17.284 ± 0.090	18.021 ± 0.117	16.073 ± 0.073			
245 6111.31	29.31			16.167 ± 0.076			
245 6114.53	32.53			16.499 ± 0.069	15.138 ± 0.044	14.656 ± 0.030	13.392 ± 0.032
245 6118.66	36.66			16.698 ± 0.084	15.296 ± 0.051	14.832 ± 0.034	13.542 ± 0.034
245 6126.88	44.88				15.426 ± 0.061	15.103 ± 0.040	13.892 ± 0.040
245 6252.90	170.90				17.610 ± 0.453	17.239 ± 0.219	16.874 ± 0.335
245 6254.70	172.70				17.641 ± 0.208	17.502 ± 0.205	17.059 ± 0.290

Note: [a]Observed phase in days with respect to the epoch of *B*-band maximum: JD = 245 6082.

is estimated as 0.92 ± 0.06. This becomes $\Delta m_{15}(B)_{\rm true} = 0.93$, after correcting for reddening. Late phase decline rate of SN 2012cg in *BVRI* bands after + 180 d estimated using linear least square fit are listed in Table 10.

The decline rate parameter $\Delta m_{15}(B)$ of both SN 2009ig and SN 2012cg is smaller than those of normal SNe Ia SN 2003du (Anupama, Sahu & Jose 2005), SN 2005cf (Pastorello et al. 2007), SN 2011fe (Vinkó et al. 2012), and comparable to that of SN 1991T (Lira et al. 1998). Similar to normal SNe Ia, in SN 2009ig and SN 2012cg, the maximum in *U*, *I* bands precede and those in the *V*, *R* bands follow the *B*-band maximum. The maximum in UV bands are also estimated and listed in Tables 9 and 10, respectively.

In Fig. 4, the optical and UV light curves of SN 2009ig and SN 2012cg have been compared with those of other well-studied SNe Ia: SN 1991T ($\Delta m_{15}(B) = 0.95$; Lira et al. 1998), SN 1999aa ($\Delta m_{15}(B) = 0.75$; Krisciunas et al. 2000), SN 2003du ($\Delta m_{15}(B) = 1.04$; Anupama et al. 2005; Stanishev et al. 2007), SN 2005cf ($\Delta m_{15}(B) = 1.11$; Pastorello et al. 2007), SN 2011fe ($\Delta m_{15}(B) = 1.07$; Vinkó et al. 2012; Brown et al. 2012), and SN 2012fr ($\Delta m_{15}(B) = 0.85$; Zhang et al. 2014). All light curves have been shifted to match their peak brightness and to the epoch of *B*-band maximum.

The *BVRI* light curves of SN 2009ig and SN 2012cg match well with other SNe with relatively smaller values of $\Delta m_{15}(B)$. In *B* band, pre-maximum rise of both SN 2009ig and SN 2012cg is faster than SN 1991T and similar to SN 2003du, SN 2005cf, and SN 2011fe. In the immediate post-maximum phase, the SNe in comparison have similar light curves, but in the exponential decline phase, they differ in brightness. SN 2009ig, SN 1991T, SN 1999aa, and SN 2012fr are brighter than SN 2012cg, SN 2003du, SN 2005cf, and SN 2011fe. In the later phase, SN 2009ig deviates from SN 1991T, SN 2012fr, and starts declining faster to become similar to SN 2012cg.

In *V* band, both SN 2009ig and SN 2012cg have light curves similar to those of SN 2003du, SN 2005cf and SN 2011fe. The width of light curve of these events is relatively narrow than SN 1991T, SN 1999aa, and SN 2012fr. In *R* and *I* bands also, the light curve of SN 2009ig/12cg is similar to normal SNe Ia. A secondary peak in *I* band characterizes the light curves of all normal and luminous SN 1991T–like SNe Ia. Both SN 2009ig and SN 2012cg show pronounced secondary maximum. As seen in *B* and *V* bands, the *R* and *I* band light curves of SN 2009ig/12cg have faster rise than SN 1991T, and similar to normal SNe in pre-maximum phase. The *UBVRI* template light curves of SN 2003du are also plotted in Fig. 3. A remarkable similarity is seen in the light curves of SN 2012cg and SN 2003du.

The light curves of all the SNe in comparison evolve differently at UV bands. SN 2009ig and SN 2012cg have slower rise in pre-

Table 7. Log of spectroscopic observations of SN 2009ig.

Date	JD[a]	Phase[b]	Range (Å)
27/08/2009	5071.46	− 9.18	3500–7800; 5200–9200
28/08/2009	5072.47	− 8.17	3500–7800; 5200–9200
01/09/2009	5076.48	− 4.16	3500–7800
05/09/2009	5080.37	− 0.27	3500–7800; 5200–9200
06/09/2009	5081.35	0.71	3500–7800; 5200–9200
07/09/2009	5082.27	1.63	3500–7800; 5200–9200
12/09/2009	5087.35	6.71	3500–7800; 5200–9200
13/09/2009	5088.35	7.71	3500–7800; 5200–9200
16/09/2009	5091.39	10.75	3500–7800; 5200–9200
20/09/2009	5095.31	14.67	3500–7800; 5200–9200
21/09/2009	5096.28	15.64	3500–7800; 5200–9200
22/09/2009	5097.36	16.72	3500–7800; 5200–9200
24/09/2009	5099.31	18.67	3500–7800; 5200–9200
26/09/2009	5101.32	20.68	3500–7800
27/09/2009	5102.42	21.78	3500–7800; 5200–9200
28/09/2009	5103.31	22.67	3500–7800; 5200–9200
30/09/2009	5105.25	24.61	3500–7800; 5200–9200
16/10/2009	5121.21	40.57	3500–7800; 5200–9200
13/11/2009	5149.19	68.55	3500–7800
14/11/2009	5150.33	69.69	3500–7800; 5200–9200
24/11/2009	5160.30	79.66	3500–7800; 5200–9200
03/12/2009	5169.10	88.46	3500–7800; 5200–9200
13/12/2009	5179.04	98.40	3500–7800; 5200–9200
14/12/2009	5180.15	99.51	3500–7800
23/12/2009	5189.15	108.51	3500–7800; 5200–9200
29/12/2009	5195.09	114.45	3500–7800; 5200–9200
11/01/2010	5208.15	127.51	3500–7800; 5200–9200
20/01/2010	5217.17	136.53	3500–7800; 5200–9200
01/02/2010	5229.13	148.49	3500–7800; 5200–9200

Note: [a]245 0000 + ; [b]Measured in days from *B*-band maximum.

Table 8. Log of spectroscopic observations of SN 2012cg.

Date	JD[a]	Phase[b]	Range (Å)
21/05/2012	6069.24	− 12.76	3500–7800; 5200–9200
22/05/2012	6070.20	− 11.80	3500–7800; 5200–9200
24/05/2012	6072.29	− 9.71	3500–7800; 5200–9200
28/05/2012	6076.25	− 5.75	3500–7800; 5200–9200
01/06/2012	6080.27	− 1.73	3500–7800
03/06/2012	6082.24	0.24	3500–7800; 5200–9200
04/06/2012	6083.26	1.26	3500–7800; 5200–9200
08/06/2012	6087.17	5.17	3500–7800; 5200–9200
12/06/2012	6091.21	9.21	3500–7800; 5200–9200
18/06/2012	6097.23	15.23	3500–7800
21/06/2012	6100.22	18.22	3500–7800; 5200–9200
26/06/2012	6105.20	23.20	3500–7800; 5200–9200
02/07/2012	6111.12	29.12	3500–7800; 5200–9200
12/07/2012	6121.18	39.18	3500–7800; 5200–9200
14/07/2012	6123.14	41.14	3500–7800; 5200–9200
16/07/2012	6125.16	43.16	3500–7800
20/07/2012	6129.17	47.17	3500–7800
06/08/2012	6146.12	64.12	3500–7800
30/11/2012	6262.48	180.48	3500–7800
09/01/2013	6302.42	220.42	3500–7800; 5200–9200
15/01/2013	6308.45	226.45	3500–7800; 5200–9200
14/02/2013	6338.48	256.48	3500–7800; 5200–9200
15/03/2013	6367.21	285.21	3500–7800; 5200–9200

[a]245 0000 + ; [b]Measured in days from *B*-band maximum.

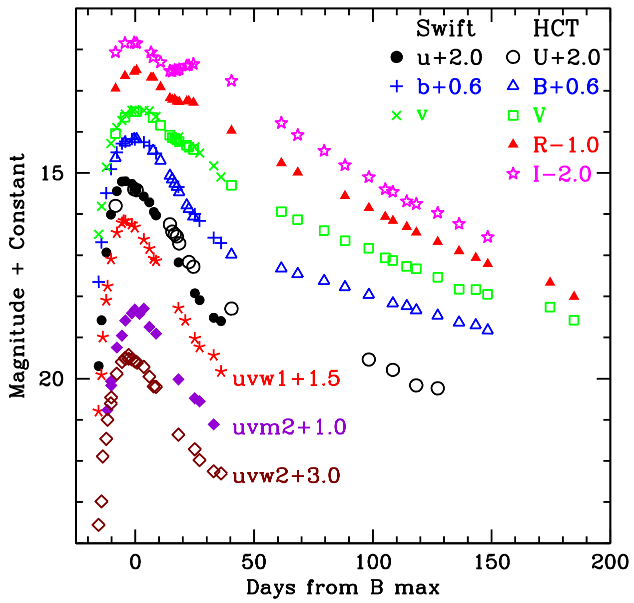

Figure 2. *UBVRI* and *Swift* UVOT light curves of SN 2009ig. The light curves have been shifted vertically by the amount indicated in the legend. The phase is measured in days from the *B*-band maximum.

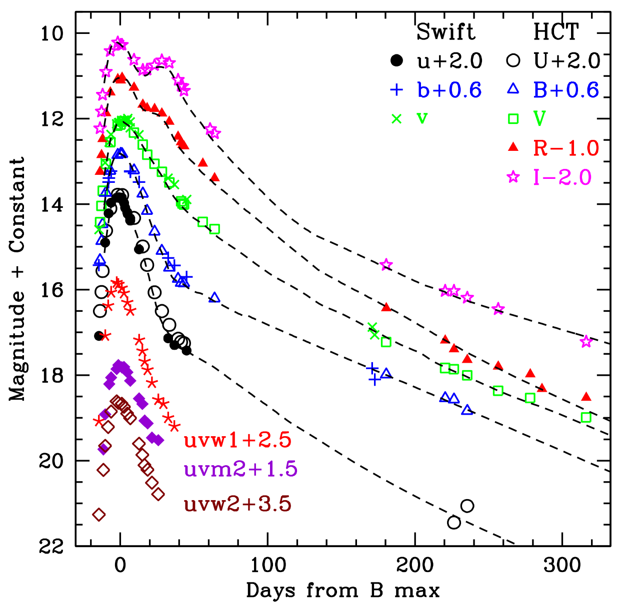

Figure 3. *UBVRI* and *Swift* UVOT light curves of SN 2012cg. The dashed lines represent template light curves of SN 2003du.

maximum phase compared to other SNe Ia (SN 2005cf/11fe/12fr). In post-maximum phase, the decline of *uvu* and *uvm*2 band light curves of SN 2009ig/12cg is slower than SN 2011fe and faster than SN 2012fr. The post-maximum evolution of *uvw*2 and *uvw*1 band light curves of SN 2009ig/12cg is similar to those of SN 2005cf and SN 2012fr.

The dereddened (*uvw*1 − *v*), (*U* − *B*), (*B* − *V*), (*V* − *R*), and (*R* − *I*) colour curves of SN 2009ig and SN 2012cg are plotted in Fig. 5. For comparison, the dereddened colour curves of some well observed SNe (used for comparing the light curves) are also plotted in the same figure. The colours of SN 2009ig and SN 2012cg are reddening corrected using the Cardelli, Clayton &

Table 9. Photometric parameters of SN 2009ig.

Data	*uvw*2	*uvm*2	*uvw*1	*U*	*B*	*V*	*R*	*I*
JD (max)[a]	77.68 ± 0.54	81.15 ± 0.51	76.72 ± 0.51	76.55 ± 0.10	80.64 ± 0.42	81.18 ± 0.61	81.83 ± 0.10	78.59 ± 0.20
$m_{\lambda}^{\max}$	16.48 ± 0.07	17.35 ± 0.15	14.66 ± 0.04	13.19 ± 0.07	13.56 ± 0.04	13.51 ± 0.03	13.52 ± 0.03	13.82 ± 0.04
$\Delta m_{15}(\lambda)$	1.09 ± 0.11	1.35 ± 0.15	1.25 ± 0.10	1.08 ± 0.07	0.91 ± 0.04	0.62 ± 0.03	0.72 ± 0.03	0.61 ± 0.05
Dec. rate[b]	5.49	7.26	8.04	6.77	6.25	5.36		
Dec. rate[c]					1.69	2.65	3.17	3.97
Dec. rate[d]					1.67	2.21	2.67	2.81
$M_{\lambda}^{\max e}$	− 16.73 ± 0.41	− 16.04 ± 0.43	− 18.48 ± 0.40	− 19.99 ± 0.41	− 19.45 ± 0.40	− 19.40 ± 0.40	− 19.33 ± 0.40	− 18.93 ± 0.40

Notes: [a]245 5000 +; Decline rate: [b]during 20–40 d; [c]during 50–100 d; [d]during 100–150 d; [e]For $\mu = 32.60$ and $E(B-V)_{\rm total} = 0.10$ mag.
Decline rate has been expressed in unit of mag (100 d)$^{-1}$ and epoch is relative to *B*-band maximum.

Table 10. Photometric parameters of SN 2012cg.

Data	*uvw*2	*uvm*2	*uvw*1	*U*	*B*	*V*	*R*	*I*
JD (max)[a]	79.73 ± 0.08	81.88 ± 0.32	79.27 ± 0.16	81.49 ± 0.07	82.00 ± 0.08	83.88 ± 0.21	83.22 ± 0.13	79.58 ± 0.16
$m_{\lambda}^{\max}$	15.12 ± 0.06	16.28 ± 0.06	13.34 ± 0.03	11.77 ± 0.06	12.22 ± 0.06	12.07 ± 0.02	12.04 ± 0.03	12.21 ± 0.03
$\Delta m_{15}(\lambda)$	0.99 ± 0.08	0.96 ± 0.09	1.28 ± 0.06	1.13 ± 0.08	0.92 ± 0.06	0.67 ± 0.03	0.67 ± 0.04	0.57 ± 0.03
Decl. rate[b]					14.57	12.93	15.11	13.14
$M_{\lambda}^{\max c}$	− 16.98 ± 0.31	− 16.18 ± 0.31	− 18.63 ± 0.30	− 20.10 ± 0.31	− 19.50 ± 0.31	− 19.45 ± 0.30	− 19.32 ± 0.30	− 18.98 ± 0.30

Note: [a]245 6000 +; [b]Decline rate after + 180 d in unit of mag (100 d)$^{-1}$; [c]For $\mu = 30.9$ and $E(B-V)_{\rm total} = 0.20$ mag.

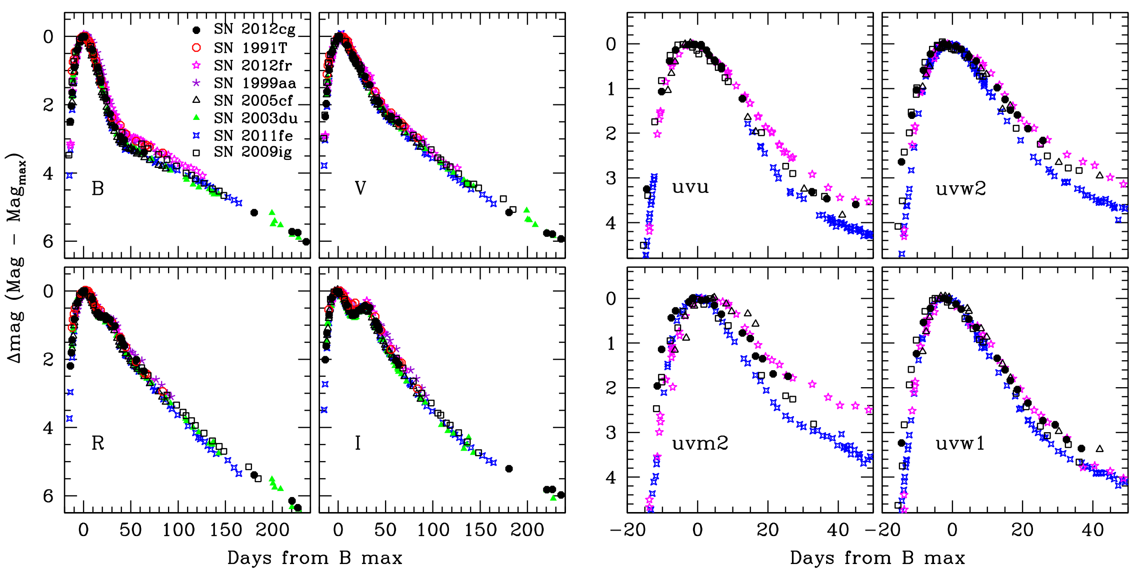

Figure 4. UV–optical light curves of SN 2009ig and SN 2012cg are compared with those of other well-studied SNe Ia. All the light curves have been shifted to match with their peak brightness and to the epoch of *B*-band maximum.

Mathis (1989) extinction law with $E(B-V)_{\rm total} = 0.10$ mag and $E(B-V)_{\rm total} = 0.20$ mag, respectively (refer Section 4.1). For other SNe used in comparison, the extinction values are taken from their respective references.

The (*uvw*1 − *v*) colour of normal SNe follows the 'V'-shape pattern (Milne et al. 2013) evolving from red to blue, reaching a minimum a few days before the optical maximum and then becoming redder again (Brown et al. 2014). For SN 2009ig and SN 2012cg, (*uvw*1 − *v*) colour reaches to minimum at ∼5 d before *B*-band maximum, similar to SN 2011fe and SN 2012fr. After this, (*uvw*1 − *v*) colour becomes redder until +30 d, then it again turns towards blue.

The (*U* − *B*) colour of SN 2012cg is bluer than SN 2009ig in early phase, but after ∼+15 d, both have similar evolution. The colour evolution of SN 2009ig/12cg follows that of SN 2003du in later phase. The (*B* − *V*) and (*V* − *R*) colours of all the SNe in comparison evolve in a similar way. These colours of SN 2009ig and SN 2012cg match well with the colours of SN 2003du. The (*R* − *I*) colour evolution of SN 2009ig/12cg is also similar to that of SN 2003du.

Foley et al. (2012b) have noticed a significant evolution in the (*B* − *V*) colour of SN 2009ig for $t < -10$ d, whereas the colour change in (*V* − *R*) and (*R* − *I*) is relatively small during this early phase. The (*B* − *V*) colour of SN 2012cg was 0.2 mag bluer than for other

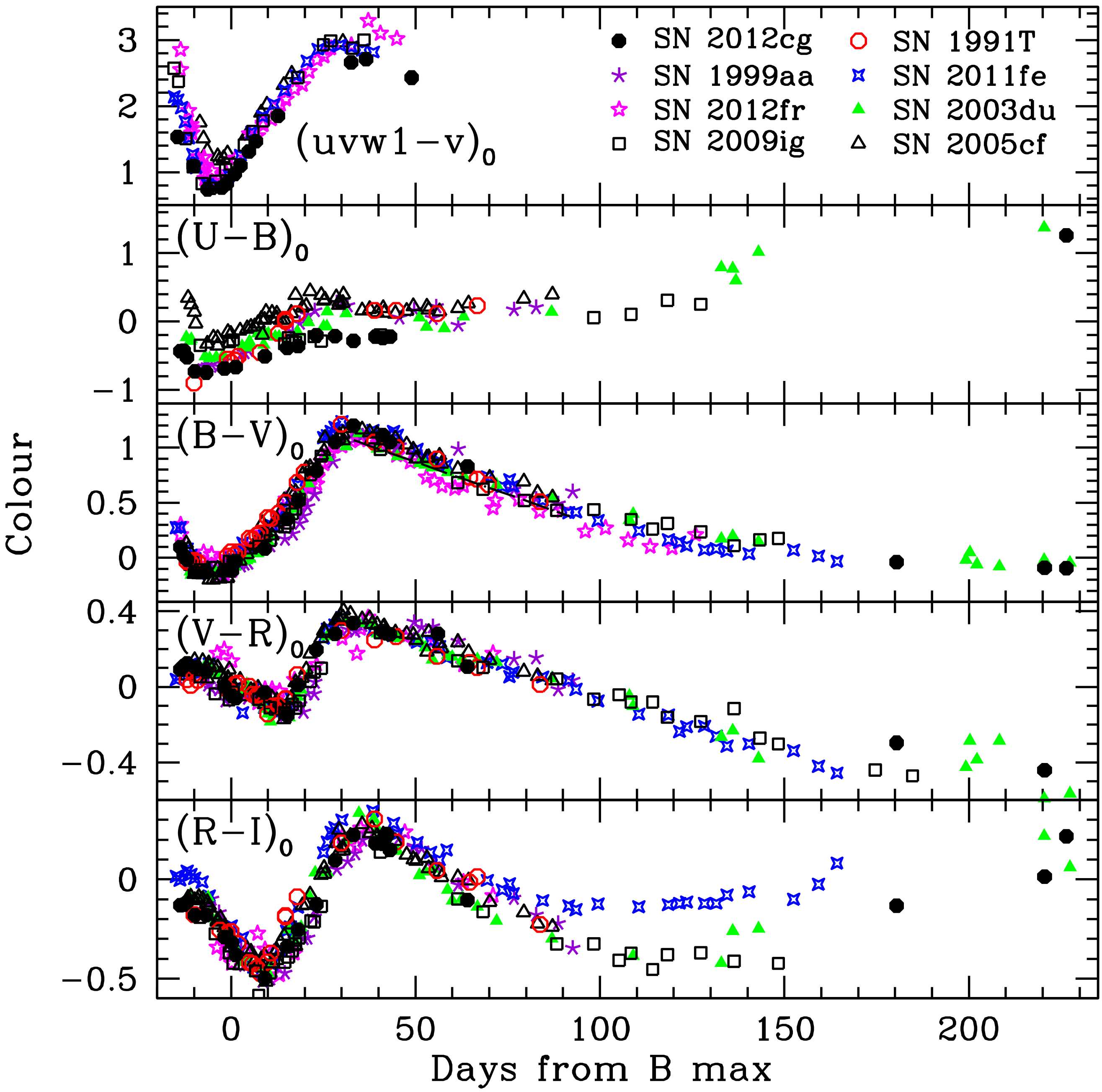

Figure 5. The $(uvw1 - v)$, $(U - B)$, $(B - V)$, $(V - R)$, and $(R - I)$ colour curves of SN 2009ig and SN 2012cg are compared with those of other well-studied SNe Ia. The dashed line drawn with the $(B - V)$ colour curve represents the *Lira–Phillips relation* (Phillips et al. 1999).

normal SN Ia at 16 d before maximum light, later on it resembles that of a typical SN Ia (Marion et al. 2016).

4 ABSOLUTE AND BOLOMETRIC LUMINOSITY

4.1 Reddening estimate

Close to maximum phase, SN 2009ig exhibits narrow Na I D absorption feature with an average EW of 0.6 ± 0.2 Å, at rest wavelength of the host galaxy. This translates to $E(B - V)_{\rm host} = 0.09$ mag (Turatto, Benetti & Cappellaro 2003). The reddening within our Galaxy in the direction of SN 2009ig is $E(B - V)_{\rm Gal} = 0.03$ mag (Schlegel, Finkbeiner & Davis 1998; Schlafly & Finkbeiner 2011) and hence the total reddening suffered by SN 2009ig is $E(B - V)_{\rm total} = 0.12$ mag.

The reddening suffered by SNe Ia can also be estimated using various empirical methods. Lira (1995), Phillips et al. (1999), and Folatelli et al. (2010) have shown that most of the SNe Ia have uniform $(B - V)$ colour evolution during 30–90 d after maximum. In Fig. 5 *Lira–Phillips relation* is drawn along with the $(B - V)$ colour evolution. The total reddening estimated using this relation is 0.11 ± 0.03 mag. Phillips et al. (1999) and Altavilla et al. (2004) have shown that the intrinsic $(B - V)$ colour of SNe Ia at maximum is correlated with $\Delta m_{15}(B)$. This method gives $E(B - V)_{\rm total} = 0.14 \pm 0.03$ mag. While total reddening of 0.08 ± 0.04

mag is estimated using method of Reindl et al. (2005). Further, to have another check the observed $(B-V)$ colour curve of SN 2009ig was dereddened until it matches with colour curves of other well-studied SNe Ia (refer Fig. 5) and we deduce a colour excess of $E(B-V)_{\mathrm{total}} = 0.10$ mag. This is in good agreement with the values derived using various empirical methods. Hence, $E(B-V)_{\mathrm{total}} = 0.10 \pm 0.04$ mag is used in the analysis of SN 2009ig. Foley et al. (2012b) have used Milky Way reddening as the total reddening for SN 2009ig. However, they have also mentioned the presence of somewhat strong Na I D absorption in their optical spectra with EW = 0.4 Å, at the redshift of the supernova, which corresponds to a total reddening of 0.09 mag (Turatto et al. 2003).

For SN 2012cg, the Galactic reddening is $E(B-V)_{\mathrm{Gal}} = 0.02$ mag (Schlegel et al. 1998; Schlafly & Finkbeiner 2011). An average EW = 1.50 ± 0.07 Å of narrow Na I D absorption feature at rest frame of the host galaxy NGC 4424 is measured in the spectra of SN 2012cg, which corresponds to colour excess of $E(B-V)_{\mathrm{host}} = 0.23 \pm 0.05$ mag (Turatto et al. 2003). The total reddening estimated using empirical relations of Phillips et al. (1999) and Altavilla et al. (2004) is 0.24 mag. While the relation of Reindl et al. (2005) gives total reddening of 0.22 mag. To match the $(B-V)$ colour evolution of other well-studied SNe Ia (refer Fig. 5), we need to deredden the $(B-V)$ colour curve of SN 2012cg by $E(B-V)_{\mathrm{total}} = 0.20$ mag. This is in good agreement with other estimates and that reported by Silverman et al. (2012) and Marion et al. (2016). For further analysis of SN 2012cg, we have used $E(B-V)_{\mathrm{total}} = 0.20 \pm 0.05$ mag.

4.2 Absolute magnitudes

Distance modulus of NGC 1015 (host galaxy of SN 2009ig) derived using Tully–Fisher relation is 32.60 ± 0.40 mag (d = 33.10 Mpc; Tully 1988). Following reddening law of Cardelli et al. (1989) and $E(B-V)_{\mathrm{total}} = 0.10$ mag, the peak absolute magnitudes of SN 2009ig in *UBVRI* bands are calculated and listed in Table 9.

Distance of NGC 4424 (host galaxy of SN 2012cg) estimated using Tully–Fisher relation is 15.2 ± 1.9 Mpc ($\mu = 30.9 \pm 0.3$ mag; Cortés, Kenney & Hardy 2008). This distance is used to estimate the peak absolute magnitudes of SN 2012cg after correcting the observed magnitudes for a total reddening of $E(B-V)_{\mathrm{total}} = 0.20$ mag (using extinction law of Cardelli et al. 1989). The derived absolute magnitudes are listed in Table 10.

The peak absolute magnitude of SNe Ia is known to correlate with $\Delta m_{15}(B)$ (Phillips et al. 1999). The relation of Folatelli et al. (2010) gives *B* band peak absolute magnitudes of SN 2009ig and SN 2012cg as −19.36 ± 0.20 mag and −19.35 ± 0.20 mag, respectively. The values are in good agreement with those obtained from the distance measurement (Tables 9 and 10).

4.3 Bolometric light curve

The bolometric luminosities of SN 2009ig and SN 2012cg were derived using the observed *UBVRI* and UV–optical magnitudes listed in Tables 3–6. The *UBVRI* magnitudes were dereddened and then converted to monochromatic fluxes using zero-points from Bessell, Castelli & Plez (1998). The UV magnitudes from *Swift* UVOT were dereddened following Brown et al. (2010) and converted to monochromatic flux using the zero-points from Poole et al. (2008). The derived fluxes for each night were integrated over the observed wavelength range. The bolometric luminosity is calculated from the integrated flux using distance of 33.1 Mpc (for SN 2009ig) and 15.2 Mpc (for SN 2012cg).

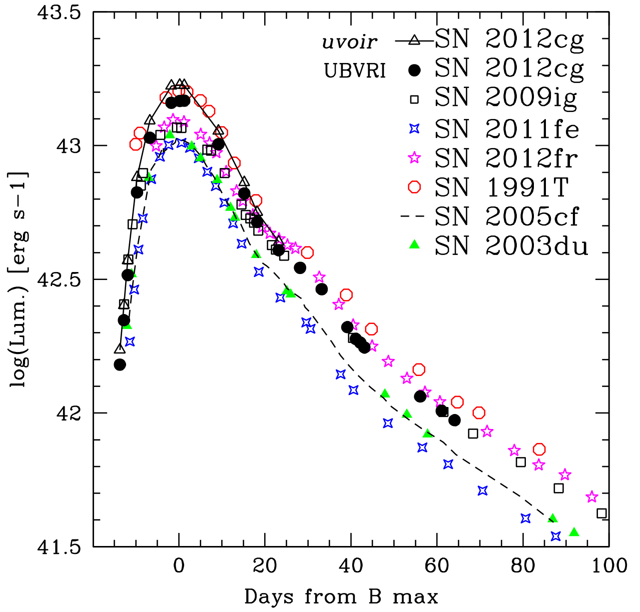

Figure 6. Bolometric light curves of SN 2009ig and SN 2012cg are plotted along with those of other well-studied SNe Ia.

The peak bolometric luminosity of SN 2012cg using only optical band is estimated as $\log L_{\mathrm{bol}}^{\mathrm{max}} = 43.17 \pm 0.11$ erg s^{-1}. This becomes $\log L_{\mathrm{bol}}^{\mathrm{max}} = 43.23 \pm 0.11$ erg s^{-1} after inclusion of UV fluxes from *Swift* UVOT data. We used NIR data from Marion et al. (2016) to estimate the flux at NIR bands, hence the *uvoir* (UV–Optical–IR) peak bolometric luminosity is obtained as $\log L_{\mathrm{bol}}^{\mathrm{max}} = 43.24 \pm 0.11$ erg s^{-1}.

For SN 2009ig, the peak is obtained as $\log L_{\mathrm{bol}}^{\mathrm{max}} = 43.07 \pm 0.16$ erg s^{-1}, when only optical *UBVRI* fluxes are integrated. While maximum bolometric luminosity obtained using UV and optical band is $\log L_{\mathrm{bol}}^{\mathrm{max}} = 43.15 \pm 0.16$ erg s^{-1}. Correction should be applied to account for contribution from NIR passbands to obtain the *uvoir* bolometric luminosity. Wang et al. (2009b) found that the NIR flux contribution shows complicated temporal evolution – after explosion NIR contribution decreases and reaches a minimum of ∼5 per cent at ∼5 d after maximum, it then rises up to ∼20 per cent at around 35 d after maximum light. At nebular phases, the NIR contribution gradually declines and drops to less than 10 per cent at ∼80 d. Adding 5 per cent flux (close to maximum) to compensate for the missing flux in NIR, the peak bolometric luminosity becomes $\log L_{\mathrm{bol}}^{\mathrm{max}} = 43.17 \pm 0.16$ erg s^{-1}.

The derived bolometric light curves of SN 2009ig and SN 2012cg are plotted in Fig. 6 and compared with those of other well-studied SNe Ia. The bolometric light curves of both SN 2009ig and SN 2012cg are brighter than SN 2003du/05cf/11fe. At the peak SN 2012cg is brighter than SN 2009ig and comparable to SN 1991T, but after ∼+20 d both SN 2009ig and SN 2012cg have similar evolution. Bolometric light curve of SN 2009ig is comparable to SN 2012fr.

4.4 Mass of nickel synthesized

The derived peak bolometric luminosity is used to estimate the mass of ^{56}Ni synthesized in the explosion. Light curve of SNe Ia is powered by the radioactive decay of ^{56}Ni, which decays to ^{56}Co and subsequently to ^{56}Fe. Arnett (1982) rule states that the peak bolometric luminosity of a type Ia SN is proportional to the instantaneous rate of energy release from radioactive decay. This can be written as

$$M_{Ni} = \frac{L_{bol}^{max}}{\alpha \dot{S}(t_R)},$$

where M_{Ni} is mass of ^{56}Ni, α is the ratio of bolometric to radioactive luminosities (near unity), and $\dot{S}(t_R)$ is the radioactivity luminosity per unit nickel mass evaluated for the rise time t_R. From Nadyozhin (1994), $\dot{S}(t_R)$ can be written as

$$\dot{S}(t_R) = \left(6.45\, e^{-(t_R/8.8d)} + 1.45\, e^{-(t_R/111.3d)}\right) \times 10^{43} \quad \mathrm{erg\,s^{-1}\,M_\odot^{-1}},$$

where 8.8 and 111.3 d are *e*-folding lifetimes (τ) of ^{56}Ni and ^{56}Co, respectively.

SN 2009ig was discovered on 2009 August 20.48. Nothing was visible at SN position on August 16.46 at a limiting mag of 18.7 mag (Kleiser et al. 2009). This gives a constrain on the rise time as $16.7 < t_R < 20.7$ d. Foley et al. (2012b) have estimated the rise time for SN 2009ig as 17 d from the pre-maximum data. Using t_R = 17 d, peak bolometric luminosity of $\log L_{bol}^{max} = 43.17$ erg s^{-1} and $\alpha = 1.2$ (Branch 1992), the mass of ^{56}Ni synthesized in the explosion of SN 2009ig is estimated as $M_{Ni} = 0.60 \pm 0.20$ M$_\odot$.

The rise time for SN 2012cg is estimated as $t_R = 17.3$ d (Silverman et al. 2012), $t_R = 18.8$ d (Marion et al. 2016), and $t_R = 19.5$ d (Shappee et al. 2018). Using $\log L_{bol}^{max} = 43.24$ erg s^{-1} and $\alpha = 1.2$, the mass of ^{56}Ni synthesized in the explosion of SN 2012cg is estimated for the above three values of rise time as $M_{Ni} = 0.68 \pm 0.17$ M$_\odot$, $M_{Ni} = 0.74 \pm 0.18$ M$_\odot$, and 0.75 ± 0.19 M$_\odot$, respectively. An average value of $M_{Ni} = 0.72 \pm 0.31$ M$_\odot$ is obtained from these.

5 SPECTRAL EVOLUTION

We obtained a series of 29 spectra of SN 2009ig from −9 to +148 d and 23 spectra of SN 2012cg from −12.8 to +285 d with respect to *B*-band maximum. The details of spectroscopic observations are given in Tables 7 and 8. Spectral evolution of SN 2009ig and SN 2012cg is presented in Figs 7, 8, 12, 13, 16 and 17. All the spectra have been corrected for reddening and redshift. Telluric lines have not been removed.

5.1 Pre-maximum phase

The early phase spectra of SNe Ia are characterized by singly ionized lines of intermediate-mass elements (IMEs) such as Si, Ca, Mg, S, O etc., superposed on blue continuum. As the spectrum evolves, they are progressively replaced by the iron group elements (IGEs). The lines in the early phase spectra of SN 2009ig and SN 2012cg are displayed and marked in Figs 7 and 8.

In the first spectrum of SN 2009ig taken at −9 d, Si II λ6355 line shows shallow and broad profile with an asymmetry in the bluer edge, which is associated with the high-velocity component of Si II line (Foley et al. 2012b; Marion et al. 2013). The effect of high-velocity component of Si II is not seen in the spectrum taken at maximum light. The presence of HVF in Ca II NIR triplet is also seen as two-component profile, with the bluer component due to the HVF. Gradually, by maximum phase, the low-velocity photospheric component becomes prominent. The Si II λ5972 is not developed in the pre-maximum spectra. A very weak signature of this line starts appearing around maximum phase. The first three spectra of SN 2009ig (−9, −8, and −4 d) show presence of doubly ionized lines

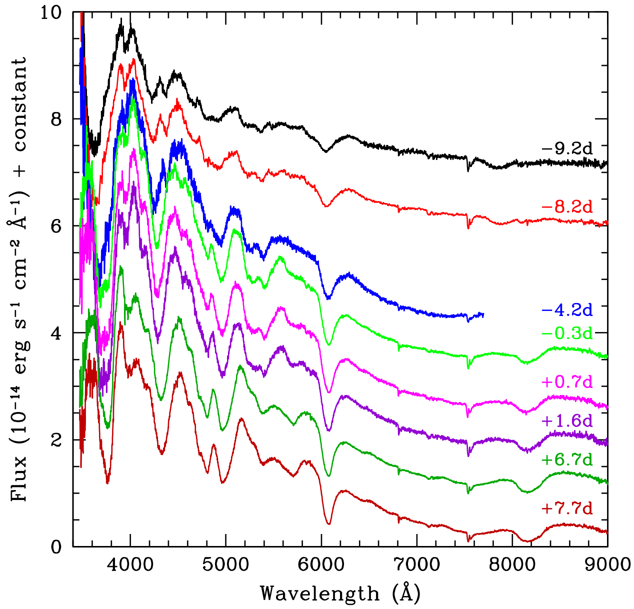

Figure 7. Spectral evolution of SN 2009ig from −9.2 to +7.7 d.

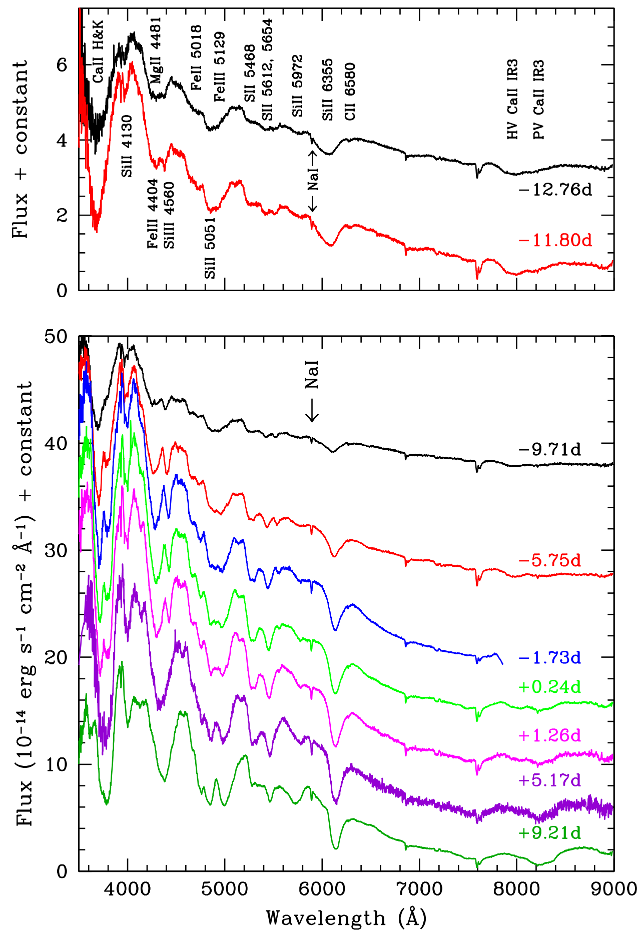

Figure 8. Spectral evolution of SN 2012cg from −12.8 to +9.2 d. Narrow Na I D feature from host galaxy is marked.

of Fe III λ4404 and Si III λ4560. The 'W' feature at ∼5200 Å due to S II λλ5468, 5654 absorption is seen in the early phase spectra. Detection of C II λ6580 was reported by Parrent et al. (2011) in the spectrum of SN 2009ig taken around −14 d. A small depression around 6200 Å was also noticed in the spectrum taken at −12 d (Foley et al. 2012b). This feature is not visible in our spectra of SN 2009ig at −9 d (Fig. 7).

The pre-maximum spectra of SN 2012cg obtained at −12.8 and −11.8 d exhibit Si II λ6355 feature skewed with respect to its minimum (Fig. 8). The red-wing of the profile has sharp rise, while blue-wing shows a gradual rise due to the presence of HVF. The HVF evolves rapidly and disappears close to maximum light. The Si II λ6355 profile is broad with triangular shape in the −9.7 d spectrum of SN 2012cg. The next spectrum taken at −5.8 d shows strengthening of most of the lines. The blend of high velocity (HV) and photospheric velocity (PV) components of Ca II H&K lines show double minima. As the spectrum ages, the HV component becomes weaker and by +9.2 d, the PV component is dominating. Similarly, HV component of Ca II NIR triplet is strong in early phase and becomes weak in post-maximum phase. The HVFs due to Ca II and Si II are common in pre-maximum spectra of SNe Ia and are seen in other species too (Mazzali et al. 2005a; Wang et al. 2009b; Childress et al. 2013; Marion et al. 2013). It is suggested that the strength of HVF increases with decreasing light curve decline rate (Childress et al. 2014; Zhao et al. 2015). SN 2009ig and SN 2012cg both being slow decliner, the HVFs are prominent. Strong Si III line is seen in the pre-maximum spectra of SN 2012cg, which disappeared by +5 d (Fig. 8). Strong Si III line and weak Si II λ5972 are indicative of hot photosphere.

There are two important features to be noticed on the wings of the Si II λ6355 in the spectra of SN 2012cg (Fig. 8). On the blue side, very sharp absorption is due to Na I D at the rest frame of the host galaxy. This sharp absorption is well inside the Si II profile in very early phase spectra (−12.8, −11.8 d), is at the edge of Si II line in the spectra taken at −9.7, −5.8 d and clearly separated from the Si II line in the spectra close to the maximum light. This shows rapid evolution of Si II λ6355 in velocity space during the pre-maximum phase. On the red edge of the Si II λ6355 line there is a small dip with decreasing strength in the spectra at −12.8, −11.8, −9.7 d. This feature is attributed to C II λ6580 from unburned material of the progenitor white dwarf.

In Fig. 9, the spectrum of SN 2009ig at −9 d and SN 2012cg at −10 d is compared with those of SN 1999aa (Garavini et al. 2004), SN 1999ac (Garavini et al. 2005), SN 2002bo (Benetti et al. 2004), SN 2003du (Anupama et al. 2005), SN 2005cf (Pastorello et al. 2007), SN 2011fe (Pereira et al. 2013), and SN 2012fr (Childress et al. 2013) at similar epoch. The spectra used for comparison are obtained from SUSPECT[2] and WISeREP.[3] All the spectra have been corrected for reddening and redshift.

Detailed comparison shows that although the spectra of all SNe Ia look similar, there are some differences in the shape and line velocities. The absorption lines are more blue shifted in the spectrum of SN 2009ig as compared to SN 2012cg. The spectra of SN 2009ig/12cg/05cf/12fr are different from others due to presence of HVFs. The Si II λ5972 and S II lines are relatively weak in the spectra of SN 2009ig/12cg/99aa/99ac than in SN 2003du/05cf/02bo/11fe.

In Fig. 10(a), spectral region around Fe III λ4404 line, in Fig. 10(b) around Si II λ6355 line, and in Fig. 10(c) around Ca II NIR triplet of

[2]http://www.nhn.ou.edu/ suspect

[3]http://www.weizmann.ac.il/astrophysics/wiserep

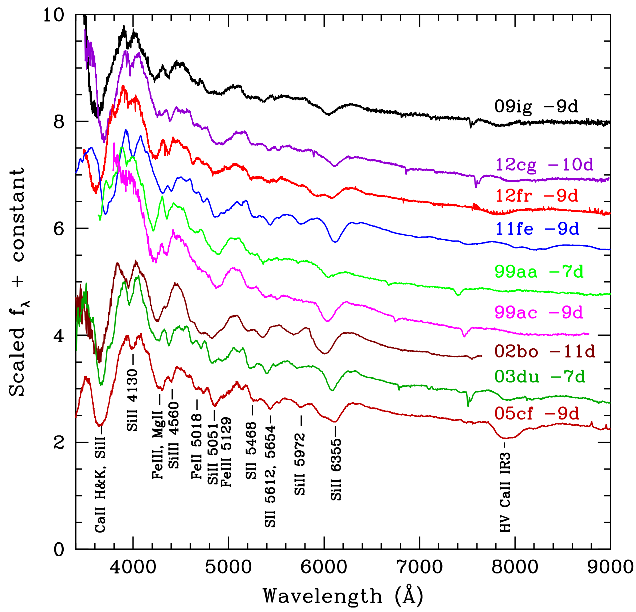

Figure 9. Pre-maximum spectrum of SN 2009ig at −9 d and SN 2012cg at −10 d are compared with those of other well-studied SNe Ia at similar epoch.

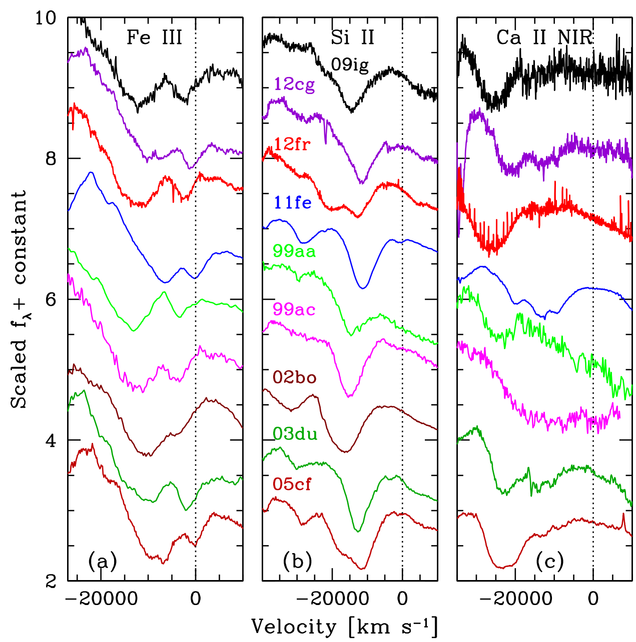

Figure 10. Comparison of line profile of Fe III λ4404, Si II λ6355, and Ca II NIR triplet in the spectra of SN 2009ig, SN 2012cg, and other SNe Ia at −9 d.

SN 2009ig, SN 2012cg is plotted in velocity space along with those of other SNe at similar epoch (∼−9 d). The line profile around Fe III λ4404 and Si III λ4560 lines in SN 2009ig and SN 1999aa is similar. Though, SN 2012cg shows strong Si III λ4560 similar to SN 2009ig, the profile around Fe III λ4404 is shallower and has a blend of two absorptions. In Fig. 10(b,c), presence of HVFs in Si II λ6355 and Ca II NIR triplet lines are clearly seen in the spectra of SN 2009ig, SN 2012cg, SN 2012fr, and SN 2005cf. Both SN 2009ig and SN 2012cg show similar skewed profile of Si II λ6355.

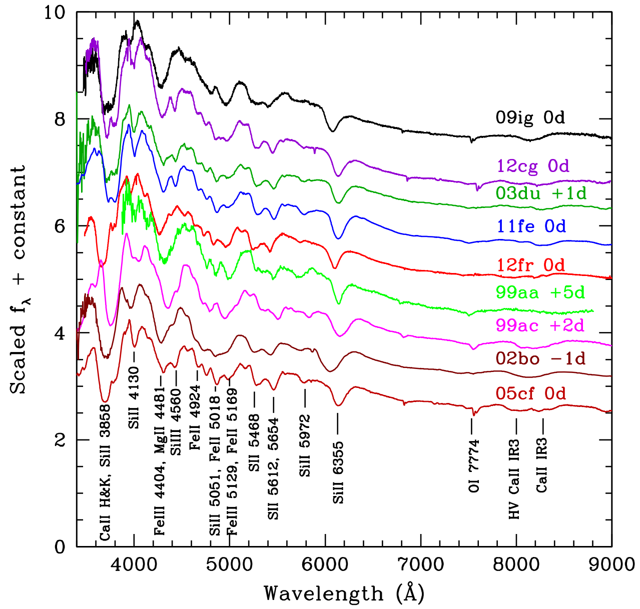

Figure 11. Comparison of spectra of SN 2009ig, SN 2012cg, and other well-studied SNe Ia at maximum.

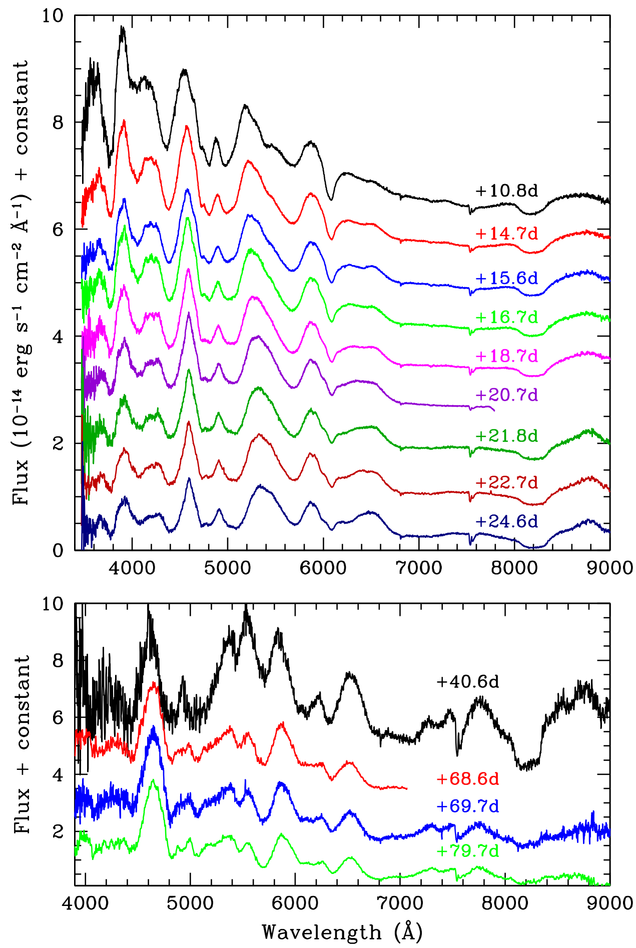

Figure 12. Spectral evolution of SN 2009ig during post-maximum phase from +11 to +80 d.

This skewed profile is very strong in SN 2012fr and SN 2005cf. Zhao et al. (2015) found that the fraction of SNe showing Si-HVFs in their sample is less compared to those having Ca-HVFs. It is also noticed that Ca-HVFs appear to be much stronger than Si-HVFs at the same phase suggesting that formation of Ca-HVFs might be easier than that of Si-HVFs.

5.2 Around maximum phase

Spectra of SN 2009ig and SN 2012cg at maximum light are compared with those of other well-studied SNe Ia at similar epoch in Fig. 11. Both SN 2009ig and SN 2012cg at maximum phase resemble spectroscopically normal SNe Ia (SN 2011fe, SN 2005cf, SN 2003du). The Fe III λ4404, Fe III λ5129, and Si III λ4560 are stronger in SN 2012cg. The Si III λ4560 line is not visible in SN 2009ig; however, Fe III λ5129 line is prominently seen similar to SN 1999aa/ac. In other SNe it is blended with Si II λ5051 and Fe II λ5018 lines. The Si II λ6355 absorption of SN 2012cg is similar to 2011fe/03du/05cf. The minima of this feature appears at similar velocity in these SNe. The Ca II H&K lines and NIR triplet profiles are similar in SN 2012cg, SN 2011fe, and SN 2003du. In SN 2009ig, the blue shift of Si II λ6355 is comparable to SN 2002bo, and higher than other SNe (refer Section 5.6).

The Si II λ5972 line is weak in the maximum light spectra of SN 2009ig and SN 2012cg as compared to normal events SN 2005cf/11fe. The ratio of strength of Si II λ5972 and Si II λ6355 known as $\mathcal{R}$(Si II) is suggested as a distance independent luminosity indicator. Its value is found to be large for dimmer objects and smaller for brighter objects. The $\mathcal{R}$(Si II) is estimated as 0.17 for SN 2009ig and 0.20 for SN 2012cg, indicating that these events are brighter, as expected from their decline rate parameter $\Delta m_{15}(B)$. The EWs of Si II λ6355 and λ5972 lines in the spectra of SN 2009ig, close to maximum are measured as 85 and 9 Å, respectively. For SN 2012cg, they are measured as 80 and 10 Å. Using these two EWs, Branch et al. (2006) have grouped SNe Ia into four subclasses. SNe 2009ig and 2012cg fall close to the region occupied by the 'Core Normal' objects.

5.3 Post-maximum phase

The post-maximum evolution of SN 2009ig from +11 to +80 d is presented in Fig. 12. The spectral evolution of SN 2009ig follows that of a normal SNe Ia. Until ∼+ 25 d the spectra are dominated by Na I, Si II, Ca II, and Fe II lines. The absorption due to Ca II H&K lines weakens in the post-maximum phase. Na I D feature becomes stronger in the region covered by Si II λ5972 line. Beyond +25 d the Si II λ6355 line is replaced by Fe II λλ6238, 6248 lines. Ca II NIR triplet remains strong with deep, broad absorption, and a pronounced emission component till ∼+41 d and afterwards it weakens. The post-maximum evolution of SN 2012cg from +15 to +64 d is shown in Fig. 13. The spectra are dominated by Fe II, Na I, and Ca II lines. Si II λ6355 gets weaker, and by +29 d only a small notch is seen. One month after maximum, O I line (though affected by telluric band) is strong.

Spectra of SN 2009ig and SN 2012cg around +40 d are compared with those of other well-studied SNe Ia in Fig. 14. At this phase spectra of both SN 2009ig and SN 2012cg are very similar to those of other SNe Ia used in comparison. Spectra of all the objects are dominated by lines due to Fe II, Na I D, and Ca II NIR triplet. They all have Ca II NIR triplet with rectangular profile (except SN 1999ac/02bo). The Fe II λ4924 and Fe II λ5018 lines are blended in SN 2009ig. These lines are visible separately in other SNe (except SN 1999ac/02bo). Fe II λ5536 line is strongest in SN 2009ig and very weak in SN 2012cg similar to SN 2003du.

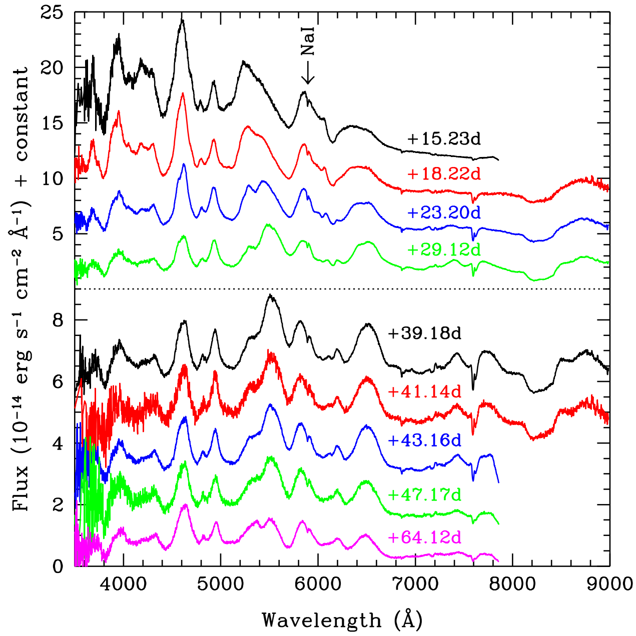

Figure 13. Spectral evolution of SN 2012cg from +15 to +64 d. Narrow Na I D feature from host galaxy is marked.

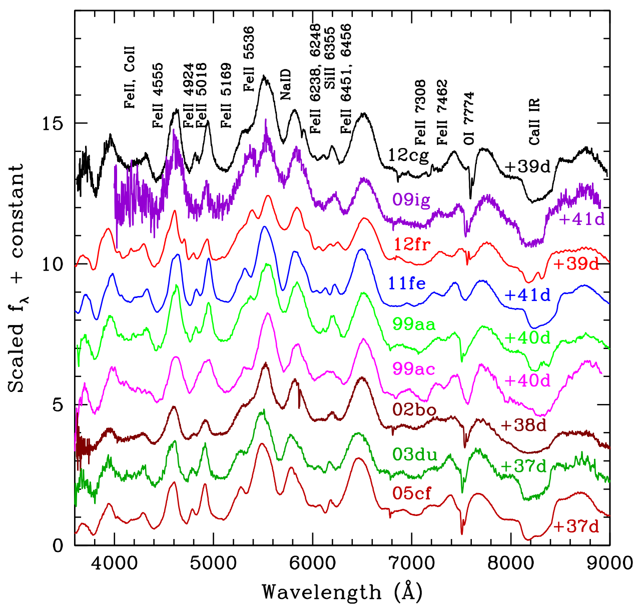

Figure 14. Comparison of spectra of SN 2009ig, SN 2012cg, and other well-studied SNe Ia at +40 d.

5.4 SYN++ fit

5.4.1 SN 2009ig

Pre-maximum spectrum of SN 2009ig at −8 d is fit with the synthetic spectrum generated using the SYN++ code (Fisher 2000; Thomas, Nugent & Meza 2011) and plotted in Fig. 15 (top panel). The synthetic spectrum with PV 14 000 km s^{-1}, blackbody temperature 16 500 K, and ions of O I, Mg II, Si II, Si III, S II, Ca II, Fe II, Fe III, matches the observed spectrum. Along with the photospheric component, additional high-velocity components of Si II at 20 500 km s^{-1} and Ca II at 25 000 km s^{-1} are included to produce the observed features. Inclusion of Co II and Ni II improves the fit at bluer part. The spectrum of SN 2009ig close to maximum matches with the synthetic spectrum having PV of 12 500 km s^{-1} and blackbody temperature of 15 500 K (Fig. 15, top panel). The ions included are O I, Mg II, Si II, Si III, S II, Ca II Fe II, Fe III, and Ni II. HV components of Si II at 17 500 km s^{-1} and Ca II at 22 000 km s^{-1} are included in the synthetic spectrum.

The spectrum of SN 2009ig at +11 d matches with synthetic spectrum having PV of 12 000 km s^{-1} and blackbody temperature of 14 000 K (Fig. 15, top panel).

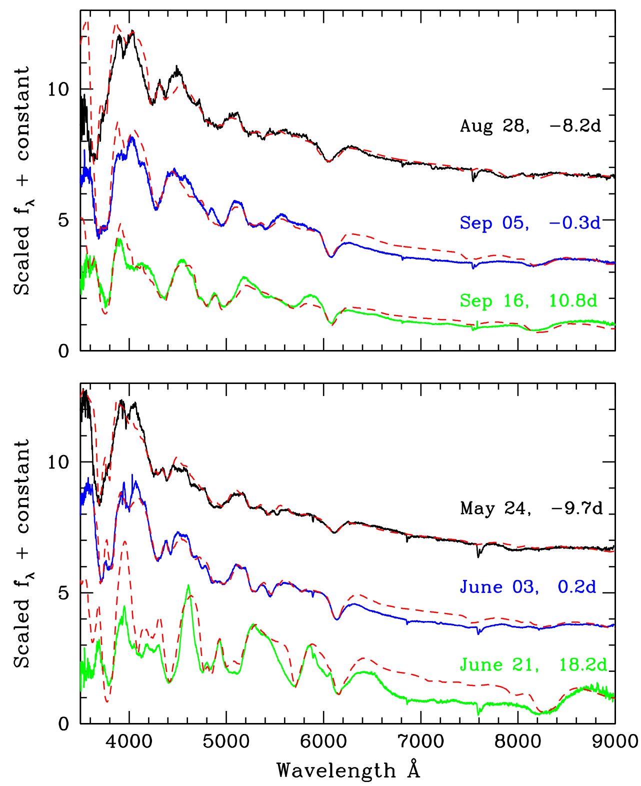

Figure 15. The synthetic spectra generated using SYN++ code are compared with the spectra of SN 2009ig (*top*) and SN 2012cg (*bottom*).

5.4.2 SN 2012cg

Pre-maximum spectrum of SN 2012cg at −9.7 d is fit with the synthetic spectrum with PV of 11 000 km s^{-1} and blackbody temperature of 15 000 K (Fig. 15 bottom panel). The ions of O I, Na I, Mg II, Si II, Si III, S II, Ca II, Fe II, and Fe III are included. Additional high-velocity components of Si II at 17 000 km s^{-1} and Ca II at 21 000 km s^{-1} are included to produce the observed features. The observed spectrum of SN 2012cg close to maximum matches with the synthetic spectrum having PV of 10 500 km s^{-1} and blackbody temperature of 15 000 K (Fig. 15, bottom panel). The same ions, as in the case of −9.7 d spectrum are included. The HV components of Si II at 12 900 km s^{-1} and Ca II at 19 000 km s^{-1} are also included. Adding Ni II improves the fit at bluer end. The observed spectrum of SN 2012cg at +18 d can be reproduced with synthetic spectrum having PV of 10 000 km s^{-1} and blackbody temperature of 10 000 K (Fig. 15, bottom panel).

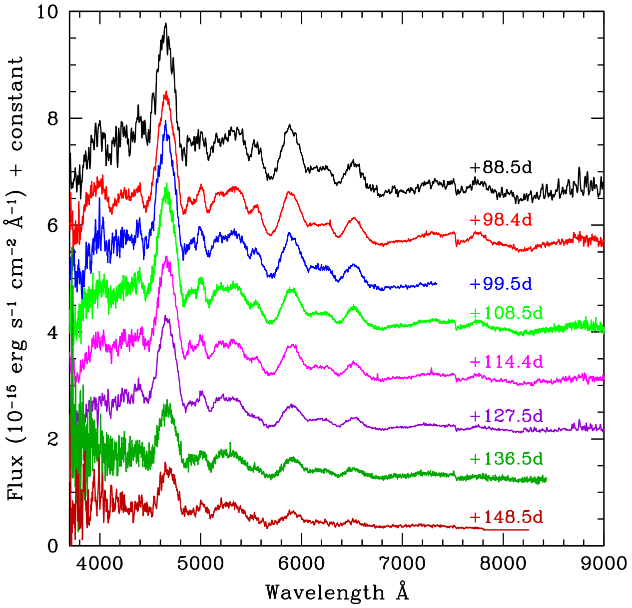

Figure 16. Spectral evolution of SN 2009ig during post-maximum phase from +88 to +148 d.

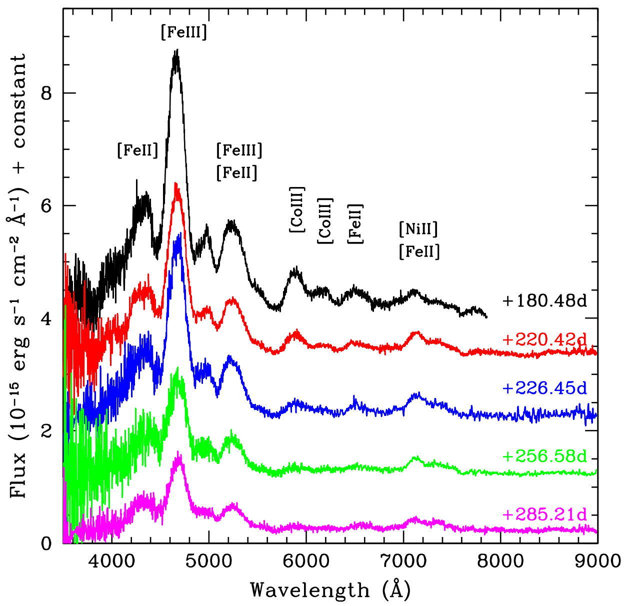

Figure 17. Spectral evolution of SN 2012cg from +180 to +285 d.

5.5 Nebular phase

As the supernova ejecta expands, photosphere moves into deeper layers and the ejecta becomes optically thin. Around six months after explosion photosphere reaches to the innermost region of the explosion, and the supernova enters into nebular phase. The spectrum is now characterized by singly and doubly ionized forbidden emission lines of IGEs (Fe, Co, Ni). The nebular spectra provide useful information about the inner region of the ejecta and are very important for understanding the explosion mechanism. Early nebular phase spectral evolution of SN 2009ig from +88.5 to +148.5 d is presented in Fig. 16. Nebular phase spectral evolution of SN 2012cg from +180.5 to +285 d is shown in Fig. 17. Nebular phase spectra of SN 2012cg are dominated by forbidden lines [Fe II], [Fe III], [Co II], [Co III], and [Ni II]. Some important features are marked in Fig. 17. The strongest feature seen in the nebular spectra is the emission at 4700 Å due to blend of several [Fe III] lines with some contribution from [Fe II] lines. The emission seen at 5200 Å arises due to comparable contributions from [Fe II] and [Fe III] lines (Mazzali et al. 2011). As the supernova ages the [Co III] lines become weaker due to decay of ^{56}Co into ^{56}Fe. Signature of nebular lines are also visible in spectra of SN 2009ig at ∼100 d, presented in Fig. 16.

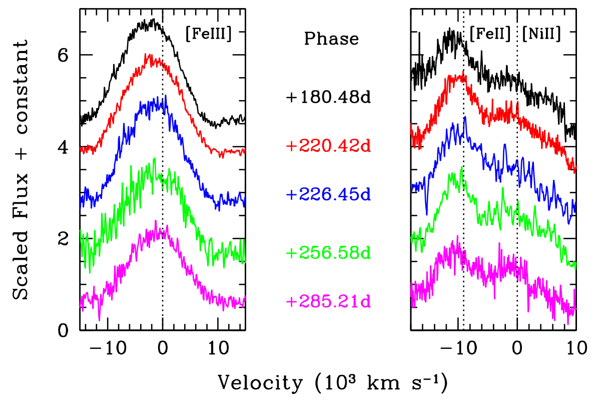

Figure 18. Nebular [Fe III] 4700 Å, [Fe II] λ7155, and [Ni II] λ7378 lines of SN 2012cg from +180.5 to +285 d are plotted in velocity space. Their rest wavelengths are shown by dotted lines.

In Fig. 18, spectral region around [Fe III] 4700 Å, [Fe II] λ7155, and [Ni II] λ7378 nebular lines of SN 2012cg from +180.5 to +285 d are plotted in velocity space. Their rest wavelengths are shown by dotted lines. The [Fe III] 4700 Å line shows blue shift till around +200 d, in the later phase the shift in line is not noticeable (refer Fig. 18, left-hand panel). This is consistent with the findings of Maeda et al. (2010a,b) and Silverman et al. (2013). The blueshift at +180.5 d is measured as ∼2400 km s^{-1}, which becomes ∼1000 km s^{-1} at + 285 d. This is in the range of [Fe III] velocities observed for other SNe Ia (Maeda et al. 2011; Silverman et al. 2013).

The [Ni II] λ7378 line is weak as compared to [Fe II] λ7155 line, in first three spectra (+180.5, +220.4, 226.4 d) of SN 2012cg (Fig. 18, right-hand panel). In the last spectrum obtained at +285 d, [Ni II] line is seen with a clear peak. In contrast to [Fe III] 4700 Å line, the [Fe II], [Ni II] lines show very little velocity evolution (Maeda et al. 2011; Silverman et al. 2013). Nebular velocity of SNe Ia is measured from the [Fe II] λ7155 and [Ni II] λ7378 emission lines. We measured an average nebular velocity of 1300 ± 200 km s^{-1} from the blueshift of [Fe II] and [Ni II] lines at +285 d spectrum of SN 2012cg.

The nebular velocity is found to correlate with the gradient of PV ($\dot{v}_{\rm Si}$) measured from Si II λ6355 line (Maeda et al. 2010a,b; Silverman et al. 2013). The objects belonging to HVG show redshift, while LVG objects generally show blueshift in the nebular [Fe II], [Ni II] lines. With $\dot{v}_{\rm Si}$= 32 km s^{-1} d^{-1}, SN 2012cg is a member of LVG subgroup and has a normal velocity (NV) of 10 000 km s^{-1} at *B*-band maximum. The nebular blueshift in SN 2012cg follows the observed trend seen in majority of objects.

The spectra of SN 2012cg at +226 and +285 d are compared with those of SN 1990N, SN 2003du, and SN 2011fe at similar epoch in Fig. 19. All the spectra are normalized to the peak of [Fe III] 4700 Å. SN 2012cg, SN 1990N, SN 2003du, and SN 2011fe have nearly similar width of [Fe III] 4700 Å line. At +226 d, SN 2012cg has

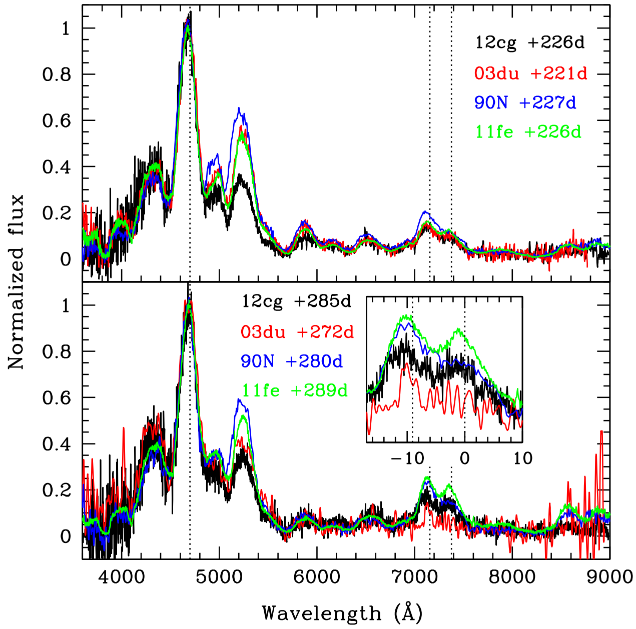

Figure 19. Comparison of spectra of SN 2012cg and other well-studied SNe Ia at nebular phase. Inset : Enlarged profile of [Fe II] λ7155 and [Ni II] λ7378 lines in velocity (10^3 km s^{-1}) space.

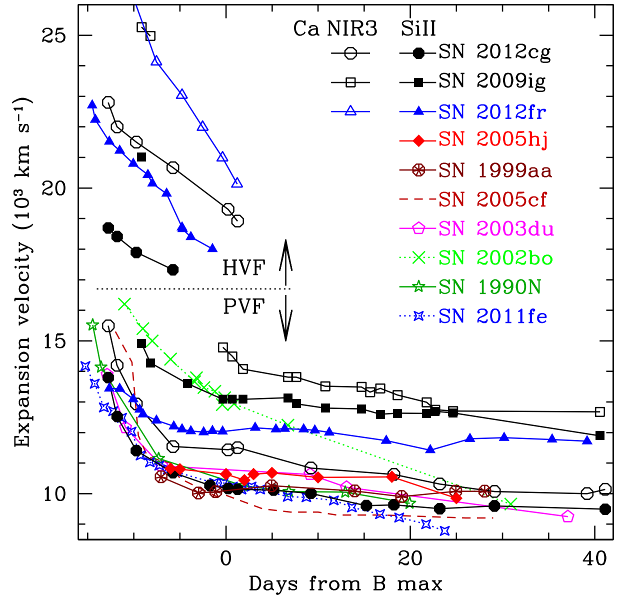

Figure 20. Photospheric velocity evolution of Si II λ6355 absorption line for SN 2009ig and SN 2012cg is compared with those of other well-studied SNe Ia (marked with PVF). Expansion velocity derived using PVF Ca II NIR triplet, and velocity measurement for HVFs seen in SN 2009ig/12cg is also displayed. High-velocity measurement in SN 2012fr is shown as a reference. Same symbols are used in displaying high velocities.

higher ratio of [Fe III] 4700 Å to [Fe II] 5200 Å as compared to other three objects used for comparison. At +285 d, both SN 2012cg and SN 2003du have comparable [Fe III]/[Fe II] ratio, which is larger than those of SN 1990N and SN 2011fe. The ratio of emission at 4700 and 5200 Å is sensitive to the ionization/excitation conditions, which gives clue to the temperature and density in the nebular ejecta (Mazzali et al. 1998). Higher [Fe III]/[Fe II] ratio suggests for higher ionization state in SN 2012cg/03du as compared to SN 2011fe/90N at late phase.

At +226 d, [Fe II] λ7155 and [Ni II] λ7378 lines have similar strength in SN 2012cg, SN 2003du, SN 2011fe, while in SN 1990N, [Fe II] λ7155 appears to be marginally stronger. At +285 d, these two lines are prominently seen in SN 2011fe, very weak in SN 2003du and with intermediate strength in SN 2012cg. Strength of [Ni II] λ7378 is similar in SN 2012cg and SN 1990N. [Ni II] λ7378 line arises due to stable ^{58}Ni. At very late phase the contribution from ^{56}Ni would be negligible because of its very short decay time. SNe with different strength of [Ni II] λ7378 line may have differing amount of stable Fe–Ni core (Maeda et al. 2010a).

5.6 Velocity and spectral parameters

The expansion velocity for SN 2009ig and SN 2012cg was derived using the absorption minimum of Si II λ6355 and Ca II NIR triplet. Continuum on both sides of the absorption minimum was identified and a Gaussian was fit to the minimum. This provides the central wavelength of the blue shifted absorption line. The early spectra of both SNe 2009ig and 2012cg show complex line profile of Si II and Ca II NIR triplet, due to presence of additional HVFs (refer Section 5.1). The HVF is blended with the photospheric component and velocity is measured by deblending both the components using packages available within IRAF. The nearby continuum around the blended lines is identified and the initial central wavelength of the lines is marked. Now the absorption profile is fit with two Gaussians using Chi-square minimization technique and the best-fitting parameters i.e. the central wavelength, equivalent width, full width half maximum etc. are determined.

The measured velocities of the HVF and photospheric components are plotted in Fig. 20. In the same figure, velocity evolution of several other well-studied SNe Ia is also shown. In general, expansion velocity of normal SNe Ia measured from Si II λ6355 line declines very rapidly before *B*-band maximum and afterwards a slow decline is seen for almost about a month. The Si II velocity of SN 2009ig at −9 d is ∼15 000 km s^{-1}, which reduced to 13 600 km s^{-1} at −4 d and it is ∼13 000 km s^{-1} at *B*-band maximum. After that there is very little evolution in the expansion velocity. Similarly, SN 2012cg in pre-maximum phase shows a fast decline in the velocity. At −12.8 d, the velocity is measured as ∼13 800 km s^{-1}, which reduced to ∼10 000 km s^{-1} at *B*-band maximum, afterwards the velocity evolution is slow, giving a plateau like appearance in post-maximum phase. The expansion velocity measured from the photospheric component of Ca II NIR triplet in the spectra of both SN 2009ig/12cg shows evolution similar to Si II line with marginally higher values. The HVF of Si II shows a higher velocity by ∼5000 km s^{-1}, and HVF of Ca II triplet has even higher velocity by 8000–9000 km s^{-1}, than their photospheric component in the earliest spectra of SN 2012cg. In SN 2009ig, HVF of Ca II NIR triplet at −9 and −8 d has velocity of ∼25 000 km s^{-1}.

Expansion velocity of SN 2009ig is comparable to SN 2002bo at maximum and in pre-maximum phase. During the post-maximum phase the expansion velocity of SN 2002bo continues to decline linearly over one month, whereas the expansion velocity of SN 2009ig attains a plateau at ∼13 000 km s^{-1}. During maximum to +10 d, the velocity gradient for SN 2009ig is estimated as 16 km s^{-1} d^{-1}. Hence, it is a member of LVG group (Benetti et al. 2005). With expansion velocity of ∼13 000 km s $^{-1}$ at maximum light, it falls in the HV type (Wang et al. 2009a). The velocity gradient of SN 2012cg during the post-maximum phase is measured as 28 km s^{-1} d^{-1}. Hence, it belongs to LVG group and with expansion velocity of 10 000 km s^{-1} close to maximum light, it falls in the 'NV' class (Wang et al. 2009a). As seen in case of SN 2012cg, the LVG SNe Ia tend to have NV at maximum phase, but SN 2009ig being a member of LVG group shows relatively higher velocity.

6 DISCUSSION

The fact that SNe Ia can be used as standardizable candles, they are important in cosmological studies (Riess et al. 1998; Perlmutter et al. 1999; Betoule et al. 2014; Riess et al. 2016; Dhawan, Jha & Leibundgut 2018). The well-sampled light curve of nearby SNe Ia, for which independent estimate of distance is available, can be used to improve the calibration of empirical relations, which in turn will improve the accuracy of distance estimated using SNe Ia as distance ladder. Further, understanding the nature of the progenitor system is very important to use them as cosmological standard candles. SNe 2009ig ($z = 0.009$) and 2012cg ($z = 0.0014$) are relatively nearby objects, discovered very early and monitored with high cadence for sufficiently long period and hence provide an opportunity to test various theoretical predictions for the DD and SD progenitor scenarios.

Though SNe Ia have been extensively used for cosmological studies, the progenitor systems and explosion mechanisms are still debated. In case of SN 2012cg, the preferred progenitor channels are discussed in great detail. The excess blue light detected in the very early phase (−16 and −15 d) was considered due to collision of the supernova ejecta with its companion star (Kasen 2010). A main-sequence star of ∼6 M$_{\odot}$ was proposed as the binary companion for the progenitor of SN 2012cg (Marion et al. 2016). An UV excess was noticed by Foley et al. (2012b) for SN 2009ig but the colours were found to be inconsistent with the interaction models. The early-excess emission could be due to multiple origins in different SN Ia subclasses. In case of luminous (SN 1991T/99aa-like) SNe Ia, early-excess emission could be powered by the radiation from a ^{56}Ni-abundant outer layer. Hence, this feature may not be a superior indicator of the SD progenitor system and care must be taken in their interpretation (Jiang et al. 2018; Stritzinger et al. 2018). Future theoretical and observational work will shed light on this issue.

Blue shifted narrow absorption features of Ca II H&K and/or Na I D, was detected in the spectra of both the objects (Sternberg et al. 2011; Foley et al. 2012a; Maguire et al. 2013). These are likely signatures of the presence of CSM in the progenitor system, due to gas outflow from the SD progenitor systems before explosion. However, the DD channel also could produce similar features. The null detection of radio emission from SN 2012cg goes against the SD channel (Chomiuk et al. 2016). In the SD scenario it is expected that the signature of H/He rich material swept up by the SN ejecta from the envelope of the companion star, should be seen in the nebular spectra of these events. The absence of H/He feature in the nebular spectrum of SNe 2009ig and 2012cg strongly disfavours a hydrogen-rich companion (Maguire et al. 2016). Theoretical binary evolution and population synthesis calculations indicated that the progenitor system of SN 2012cg involves likely an MS donor in SD scenario or a carbon–oxygen WD donor in DD scenario (Liu & Stancliffe 2016), however, both scenarios are in conflict with the observational findings (Maguire et al. 2016; Marion et al. 2016). Further, the radius of the Roche lobe overflowing companion was constrained to be <0.24 R$_{\odot}$, using nebular spectrum and X-ray data along with the prediscovery image, ruling out a non-degenerate companion and strongly support a DD progenitor for SN 2012cg (Shappee et al. 2018).

The spectroscopic data of both the objects obtained during pre-maximum phase revealed strong HVFs (Section 5.1). The HVFs have been observed more commonly for Ca II and Si II lines (Mazzali et al. 2005a; Wang et al. 2009b; Childress et al. 2013, 2014; Silverman et al. 2015; Zhao et al. 2015). In case of SN 2009ig the HVFs were identified in several other species also (Marion et al. 2013). The strength of the HVFs is found to be correlated with various parameters like decline rate, colour, expansion velocity, properties of the host galaxies etc. (Childress et al. 2014; Pan et al. 2015; Silverman et al. 2015; Zhao et al. 2015). However, the physical origin of these HVFs is still unclear. Abundance enhancements, density enhancements, and ionization effects have been proposed to explain HVFs, which are linked with the explosion itself or may result from the interaction between ejecta and nearby CSM (Gerardy et al. 2004; Mazzali et al. 2005a,b; Tanaka et al. 2006, 2008). Mulligan & Wheeler (2017) have shown that the HVF in Ca II NIR triplet is better explained by the supernova model interacting with a shell of mass 0.005 M$_{\odot}$. The physical origin and composition of the shell is not fully known; however, some explosion models that envoke surface detonation of a helium envelope around the progenitor or models that include accretion on to the progenitor could form such shells.

Both SNe 2009ig/12cg show long velocity plateau. Similar feature was seen in SN 2005hj (Quimby, Höflich & Wheeler 2007) and SN 2012fr (Childress et al. 2013). Long velocity plateaus in these SNe were explained involving a shell-like density structures. Shell-like density structures produce velocity plateau in a natural way. To form this structure, interaction of rapidly expanding ejecta with a surrounding overlying material is required, which could be formed in models like pulsating delayed detonation model and mergers/tamped detonation models (Khokhlov, Mueller & Hoeflich 1993). Dense layer in these models remains optically thick for some time, resulting in a plateau in the Si II velocity.

Observations of SNe Ia at nebular phase could also be useful in understanding explosion physics. Graur et al. (2016) observed SN 2012cg during 570–1055 d after maximum light and found that the light curves at late phase are consistent with energy contribution from the reprocessing of electrons and X-rays emitted by the decay of ^{57}Co. This gives an evidence that apart from ^{56}Ni, radioactive ^{57}Ni is also produced in SN Ia explosions and the high ^{57}Co/^{56}Co ratio points towards a near Chandrasekhar mass progenitor. However, their results could also be explained by a light echo 14 mag fainter than SN 2012cg at peak.

Though the main observable photometric properties namely ($\Delta m_{15}(B)$, B band peak absolute magnitude, and mass of ^{56}Ni) of SNe 2009ig and 2012cg are similar, they do exhibit differences in some other properties. The very early phase (∼−16 to −15 d) light curve of SN 2012cg showed blue excess, a possible hint of interaction with a companion star, but SN 2009ig did not exhibit convincing blue excess during the comparable epoch. Both the objects belong to LVG subclass of type Ia supernovae; however, SN 2009ig showed higher velocities of Si II and Ca II NIR triplet than SN 2012cg. Both the objects showed C II features during early phase, the C II feature was seen in SN 2012cg beyond −9 d, whereas in SN 2009ig it disappeared earlier than −9 d. This indicates that in the outer layer (or in the velocity space) of the ejecta unburned C is more extended in SN 2012cg than in SN 2009ig. In the delayed detonation explosion model of type Ia supernova this may point towards early deflagration to detonation transition in SN 2009ig than SN 2012cg.

7 SUMMARY

Extensive photometry and spectroscopic analyses of two nearby normal SNe Ia SN 2009ig and SN 2012cg are presented. Both SN 2009ig and SN 2012cg are slow decliner, their decline rate parameter is estimated as $\Delta m_{15}(B)_{\rm true} = 0.92 \pm 0.04$ and 0.93 ± 0.06, respectively. They fall towards luminous side of normal SNe Ia ($M_B^{\rm max} = -19.45 \pm 0.40$ mag for SN 2009ig and -19.50 ± 0.31 mag for SN 2012cg). Peak bolometric luminosities ($\log L_{\rm bol}^{\rm max}$) of these events are estimated as 43.17 ± 0.16 erg s^{-1} and 43.24 ± 0.11 erg s^{-1}. The mass of ^{56}Ni synthesized in the explosion is 0.60 ± 0.20 and 0.72 ± 0.31 M$_{\odot}$. Their early spectra are characterized by strong Fe III, Si III, and weak Si II λ5972 line suggesting for hot photosphere. Additional high-velocity components of Si II and Ca II lines are seen in the pre-maximum phase.

The post-maximum velocity evolution shows a plateau like phase with velocities ~13 000 km s^{-1} for SN 2009ig and ~10 000 km s^{-1} for SN 2012cg. Both events show spectral evolution similar to normal SNe Ia and fall in LVG and Core Normal subgroup. Both have smaller strength ratio ($\mathcal{R}$(Si II) = 0.17 for SN 2009ig and 0.20 for SN 2012cg) consistent with smaller $\Delta m_{15}(B)$. Well sampled photometric and spectroscopic data spanning from early to very late phase make these two events as best-studied templates for future SNe Ia studies.

SN 2009ig and SN 2012cg, both are among few young SNe Ia for which earliest observations with dense coverage are available. Their early observation made possible to measure the explosion time precisely. The extensive data set of SN 2012cg in X-ray, UV, Optical, and IR, provides an opportunity to explore the ejecta companion/CSM interaction and various explosion scenario. Objects like SN 2009ig and SN 2012cg will serve as basis for understanding the explosion physics through observational signature and theoretical modelling.

ACKNOWLEDGEMENTS

We thank the referee for going through the manuscript carefully and providing constructive comments, which improved the manuscript. We thank Dr. Masaomi Tanaka for fruitful discussion during revision of the manuscript. NKC is thankful to the Director and Dean of IIA, Bangalore for local hospitality and facilities provided. DKS and GCA acknowledge the DST-JSPS grant DST/INT/JSPS/P-281/2018 and BRICS grant, DST/IMRCD/BRICS/PilotCall1/MuMeSTU/2017(G). We are thankful to the staff at IAO for their assistance during the observations and to all the observers of the 2-m HCT (IAO-IIA), who kindly provided part of their observing time for supernova observations. This work has made use of public data in the *Swift* data archive and the NASA/IPAC Extragalactic Database (NED) which is operated by Jet Propulsion Laboratory, California Institute of Technology, under contract with the National Aeronautics and Space Administration. We acknowledge the use of Online Supernova Spectrum Archive (SUSPECT), initiated and maintained at the Homer L. Dodge Department of Physics and Astronomy, University of Oklahoma; and Weizmann Interactive Supernova Data Repository (WISeREP) maintained by the Weizmann Institute of Science computing center.

REFERENCES

Altavilla G. et al., 2004, MNRAS, 349, 1344
Anupama G. C., Sahu D. K., Jose J., 2005, A&A, 429, 667
Arnett W. D., 1982, ApJ, 253, 785
Benetti S. et al., 2004, MNRAS, 348, 261
Benetti S. et al., 2005, ApJ, 623, 1011
Bessell M. S., Castelli F., Plez B., 1998, A&A, 337, 321
Betoule M. et al., 2014, A&A, 568, A22
Bloom J. S. et al., 2012, ApJ, 744, L17
Branch D. et al., 2006, PASP, 118, 560
Branch D., 1992, ApJ, 392, 35
Brown P. J. et al., 2009, AJ, 137, 4517
Brown P. J. et al., 2010, ApJ, 721, 1608
Brown P. J. et al., 2012, ApJ, 753, 22
Brown P. J. et al., 2014, ApJ, 787, 29
Cao Y. et al., 2015, Nature, 521, 328
Cardelli J. A., Clayton G. C., Mathis J. S., 1989, ApJ, 345, 245
Cenko S. B. et al., 2012, Astron. Telegram, 4115, 1
Childress M. J. et al., 2013, ApJ, 770, 29
Childress M. J., Filippenko A. V., Ganeshalingam M., Schmidt B. P., 2014, MNRAS, 437, 338
Chomiuk L. et al., 2016, ApJ, 821, 119
Cortés J. R., Kenney J. D. P., Hardy E., 2008, ApJ, 683, 78
Dessart L., Blondin S., Hillier D. J., Khokhlov A., 2014, MNRAS, 441, 532
Dhawan S., Jha S. W., Leibundgut B., 2018, A&A, 609, A72
Fisher A. K., 2000, PhD thesis, The University of Oklahoma
Folatelli G. et al., 2010, AJ, 139, 120
Foley R. J. et al., 2012a, ApJ, 752, 101
Foley R. J. et al., 2012b, ApJ, 744, 38
Garavini G. et al., 2004, AJ, 128, 387
Garavini G. et al., 2005, AJ, 130, 2278
Gehrels N. et al., 2004, ApJ, 611, 1005
Gerardy C. L. et al., 2004, ApJ, 607, 391
Graur O., Zurek D., Shara M. M., Riess A. G., Seitenzahl I. R., Rest A., 2016, ApJ, 819, 31
Hillebrandt W., Niemeyer J. C., 2000, ARA&A, 38, 191
Hosseinzadeh G. et al., 2017, ApJ, 845, L11
Howell D. A., 2011, Nat. Commun., 2, 350
Hoyle F., Fowler W. A., 1960, ApJ, 132, 565
Iben Jr. I., Tutukov A. V., 1984, ApJS, 54, 335
Jiang J. A. et al., 2017, Nature, 550, 80
Jiang J. A., Doi M., Maeda K., Shigeyama T., 2018, ApJ, 865, 149
Kasen D., 2010, ApJ, 708, 1025
Kent B. R. et al., 2008, AJ, 136, 713
Khokhlov A., Mueller E., Hoeflich P., 1993, A&A, 270, 223
Kleiser I., Cenko S. B., Li W., Filippenko A. V., 2009, Central Bureau Electronic Telegrams, Vol. 1918. IAU, Smithsonian Astrophysical Observatory, Cambridge, p. 1
Krisciunas K., Hastings N. C., Loomis K., McMillan R., Rest A., Riess A. G., Stubbs C., 2000, ApJ, 539, 658
Landolt A. U., 1992, AJ, 104, 340
Levanon N., Soker N., 2017, MNRAS, 470, 2510
Levanon N., Soker N., García-Berro E., 2015, MNRAS, 447, 2803
Lira P. et al., 1998, AJ, 115, 234
Lira P., 1995, Master's thesis, Univ. Chile
Liu Z. W., Stancliffe R. J., 2016, MNRAS, 459, 1781
Maeda K., Terada Y., 2016, Int. J. Mod. Phys. D, 25, 1630024
Maeda K., Taubenberger S., Sollerman J., Mazzali P. A., Leloudas G., Nomoto K., Motohara K., 2010a, ApJ, 708, 1703
Maeda K. et al., 2010b, Nature, 466, 82
Maeda K. et al., 2011, MNRAS, 413, 3075
Maeda K., Jiang J.-a., Shigeyama T., Doi M., 2018, ApJ, 861, 78
Maguire K. et al., 2013, MNRAS, 436, 222
Maguire K., Taubenberger S., Sullivan M., Mazzali P. A., 2016, MNRAS, 457, 3254
Maoz D., Mannucci F., Nelemans G., 2014, ARA&A, 52, 107
Marion G. H. et al., 2013, ApJ, 777, 40
Marion G. H. et al., 2016, ApJ, 820, 92
Mazzali P. A., Cappellaro E., Danziger I. J., Turatto M., Benetti S., 1998, ApJ, 499, L49
Mazzali P. A. et al., 2005a, ApJ, 623, L37

Mazzali P. A., Benetti S., Stehle M., Branch D., Deng J., Maeda K., Nomoto K., Hamuy M., 2005b, MNRAS, 357, 200
Mazzali P. A., Maurer I., Stritzinger M., Taubenberger S., Benetti S., Hachinger S., 2011, MNRAS, 416, 881
Miller A. A. et al., 2018, ApJ, 852, 100
Milne P. A., Brown P. J., Roming P. W. A., Bufano F., Gehrels N., 2013, ApJ, 779, 23
Mulligan B. W., Wheeler J. C., 2017, MNRAS, 467, 778
Munari U., Henden A., Belligoli R., Castellani F., Cherini G., Righetti G. L., Vagnozzi A., 2013, New Astron., 20, 30
Nadyozhin D. K., 1994, ApJS, 92, 527
Navasardyan H., Cappellaro E., Benetti S., 2009, Central Bureau Electronic Telegrams, Vol. 1918. IAU, Smithsonian Astrophysical Observatory, Cambridge, p. 2
Noebauer U. M., Kromer M., Taubenberger S., Baklanov P., Blinnikov S., Sorokina E., Hillebrandt W., 2017, MNRAS, 472, 2787
Nugent P. E. et al., 2011, Nature, 480, 344
Pan Y. C., Sullivan M., Maguire K., Gal-Yam A., Hook I. M., Howell D. A., Nugent P. E., Mazzali P. A., 2015, MNRAS, 446, 354
Parrent J. T. et al., 2011, ApJ, 732, 30
Pastorello A. et al., 2007, MNRAS, 376, 1301
Pereira R. et al., 2013, A&A, 554, A27
Perlmutter S. et al., 1999, ApJ, 517, 565
Phillips M. M., Lira P., Suntzeff N. B., Schommer R. A., Hamuy M., Maza J., 1999, AJ, 118, 1766
Piro A. L., Morozova V. S., 2016, ApJ, 826, 96
Piro A. L., Chang P., Weinberg N. N., 2010, ApJ, 708, 598
Poole T. S. et al., 2008, MNRAS, 383, 627
Quimby R., Höflich P., Wheeler J. C., 2007, ApJ, 666, 1083
Rabinak I., Livne E., Waxman E., 2012, ApJ, 757, 35
Reindl B., Tammann G. A., Sandage A., Saha A., 2005, ApJ, 624, 532
Riess A. G. et al., 1998, AJ, 116, 1009
Riess A. G. et al., 2016, ApJ, 826, 56
Roming P. W. A. et al., 2005, Space Sci. Rev., 120, 95
Schlafly E. F., Finkbeiner D. P., 2011, ApJ, 737, 103
Schlegel D. J., Finkbeiner D. P., Davis M., 1998, ApJ, 500, 525
Shappee B. J., Piro A. L., Stanek K. Z., Patel S. G., Margutti R. A., Lipunov V. M., Pogge R. W., 2018, ApJ, 855, 6
Silverman J. M., Vinkó J., Marion G. H., Wheeler J. C., Barna B., Szalai T., Mulligan B. W., Filippenko A. V., 2015, MNRAS, 451, 1973
Silverman J. M. et al., 2012, ApJ, 756, L7
Silverman J. M. et al., 2013, ApJS, 207, 3
Stanishev V. et al., 2007, A&A, 469, 645
Sternberg A. et al., 2011, Science, 333, 856
Stritzinger M. D. et al., 2018, ApJ, 864, L35
Tanaka M., Mazzali P. A., Maeda K., Nomoto K., 2006, ApJ, 645, 470
Tanaka M. et al., 2008, ApJ, 677, 448
Thomas R. C., Nugent P. E., Meza J. C., 2011, PASP, 123, 237
Tully R. B., 1988, Nearby Galaxies Catalog. Cambridge Univ. Press, Cambridge
Turatto M., Benetti S., Cappellaro E., 2003, in Hillebrandt W., Leibundgut B., eds, Proc. ESO/MPA/MPE Workshop, From Twilight to Highlight: The Physics of Supernovae. Springer, Berlin, p. 200
Vinkó J. et al., 2012, A&A, 546, A12
Wang X. et al., 2009a, ApJ, 699, L139
Wang X. et al., 2009b, ApJ, 697, 380
Webbink R. F., 1984, ApJ, 277, 355
Whelan J., Iben Jr. I., 1973, ApJ, 186, 1007
Zhang J. J., Wang X. F., Bai J. M., Zhang T. M., Wang B., Liu Z. W., Zhao X. L., Chen J. C., 2014, AJ, 148, 1
Zhao X. et al., 2015, ApJS, 220, 20

This paper has been typeset from a TEX/LATEX file prepared by the author.